Universidad Autónoma de San Luis Potosí

Movimiento de gotas de agua emulsificadas espontáneamente sobre una superficie fuera de equilibrio

Tesis que para obtener el grado de:

Doctora en Ciencias Interdisciplinarias

Presenta

María de Jesús Martínez López

Línea de Investigación:
Física de Materiales

Director de tesis   :   Dr. Bernardo José Luis Arauz Lara

Comité evaluador   :   Dr. Said Eduardo Aranda Espinoza

                              Dr. Juan Rodrigo Vélez Cordero

                              Dr. Roberto Sánchez Olea

                              Dra. Perla Xochil Viveros Méndez

Universidad Autónoma de San Luis Potosí

Movement of spontaneously emulsified water droplets on an out-of-equilibrium surface

Thesis submitted in partial fulfilment of the requirements for the degree of:

Doctora en Ciencias Interdisciplinarias

by

María de Jesús Martínez López

Investigation line:
Materials Physics

Thesis Advisor	:	Dr. Bernardo José Luis Arauz Lara
Examiners	:	Dr. Said Eduardo Aranda Espinoza
		Dr. Juan Rodrigo Vélez Cordero
		Dr. Roberto Sánchez Olea
		Dra. Perla Xochil Viveros Méndez

María de Jesús Martínez López: *Movement of spontaneously emulsified water droplets on an out-of-equilibrium surface*, © February 28, 2023

RESUMEN

La comprensión teórica y práctica de fenómenos interfaciales es de gran importancia debido a que sus aplicaciones se extienden a diferentes ámbitos de la física, química y biología, por ejemplo: en la catálisis heterogénea, detergencia, lubricación, adhesión, flotación de minerales, formación y estabilidad de emulsiones, etc. Particularmente, las emulsiones son dispersiones coloidales de dos líquidos inmiscibles (por ejemplo el agua y el aceite), llamadas fase discontinua y continua, es decir, el líquido que forma las gotas y el medio circundante, respectivamente. El sistema está estabilizado por un tensoactivo que disminuye la tensión interfacial y, por lo tanto, disminuye la energía libre para la formación de gotas. Por lo general, si los líquidos están en equilibrio, para formar la emulsión es necesario suministrar energía al sistema, ya sea mecánica, térmica o de ultrasonido. De manera que la energía de entrada permite dispersar la fase discontinua en la fase continua aumentando el área interfacial a través de la formación de gotas. Por otro lado, si los dos líquidos inmiscibles no están en equilibrio, los gradientes en el potencial químico entre las fases pueden generar valores negativos de energía libre y la emulsificación se produce espontáneamente es decir, se observan gotas, sin la ayuda de agentes externos que suministren energía. La emulsificación espontánea es de especial interés en el desarrollo de métodos eficientes de ahorro de energía para la fabricación de emulsiones, en una serie de aplicaciones en la industria como las de alimentos, productos farmacéuticos, cosméticos, pinturas, etc.

En este trabajo no se estudiaron las causas de la emulsificación espontánea, que son interesantes por sí mismas. El objetivo fue estudiar experimentalmente el movimiento de especies coloidales en una superficie fuera de equilibrio térmico, en el sistema agua/glicerol/dodecano/span 80. La interfaz es un menisco convexo, que aparece cuando se coloca la mezcla de agua+glicerol sobre la mezcla de dodecano+span 80 en una celda de acero inoxidable compuesta por dos agujeros cilíndricos concéntricos. El proceso de emulsificación espontánea sucede en la interfaz, debido a la naturaleza del tensoactivo, se observaron gotas constituidas por la fase acuosa, las cuales se generan espontaneamente y constituyen las especies coloidales analizadas. La presencia del glicerol alenta el movimiento de las gotas, de manera que en la región de observación se obtienen trayectorias más largas

que las que se obtendrían sin la presencia del glicerol. Las gotas de agua se mueven, hacia la parte más baja del menisco, unidas a la interfaz, mientras continuan creciendo de tamaños submicrométricos hasta unos cuantos micrómetros. Al llegar al fondo del menisco, las gotas sedimentan y forman una estructura cristalina. A pesar de la naturaleza dinámica del proceso, con la interfaz y las gotas cambiando produciendo heterogeneidades en el sistema, no se observó difusión anómala. La difusión de las gotas tiene un componente Browniano bien identificado con una distribución Gausiana de pasos debida a la agitación térmica del medio en el que se encuentran y una velocidad de deriva asociada al efecto de la gravedad sobre las gotas y sobre la interfaz. Además, se observaron cambios temporales en el comportamiento de las gotas, como la disminución del número de gotas que se mueven hacia la estructura cristalina y la disminución de su velocidad.

Por otro lado, para evaluar cualitativamente la capacidad de encapsulamiento en la emulsificación espontánea se realizaron experimentos en una celda horizontal de vidrio con los líquidos inmiscibles sobre el mismo plano de observación. La interfaz era aproximadamente plana, en la fase acuosa se agregaron las especies a evaluar: moléculas fluorescentes (dextran-rodamina y dextran-fluoresceína), nanocristales $CdSe/ZnS$ y nano-partículas coloidales. Por otro lado, en la fase oleosa se agregó el span 80. En esta configuración, las gotas formadas por emulsificación espontánea se alejan de la interfaz por difusión, algunas contenían las especies de prueba, por lo que se podía evaluar si la especie de prueba atravesaba o no la interfaz. En el caso de las moléculas fluorescentes, se observó que todas las gotas formadas contenían la especie de prueba, mientras que en el caso de los nano-cristales $CdSe/ZnS$ y de las nano-partículas coloidales, el autoensamble de las especies de prueba en la interfaz hizo menos eficiente el encapsulamiento, que se lograba solo en unas gotas y después de varios días de observación. Debido a la naturaleza dinámica de la interfaz y al autoensamble coloidal se encontró además, que las gotas formaban una gran variedad de estructuras.

ABSTRACT

Emulsions are colloidal dispersions of two immiscible liquids, such as water and oil, stabilized by a third phase, called surfactant. This third phase is usually constituted by amphiphilic molecules that tend to concentrate at the interface and reduce surface tension. Commonly it is necessary to supply external energy to the system to disperse one liquid in another, to overcome the viscous resistance and produce such metastable mixtures. But one exception is the special case where spontaneous emulsification occurs. Spontaneous emulsification consists of placing two immiscible liquids in contact that will start an emulsification process without supplying external energy to the system. Spontaneous emulsification is of particular interest in the development of efficient energy-saving methods for the manufacture of emulsions in a number of industry applications such as food, pharmaceuticals, cosmetics, paints, etc.

In this work, the causes of spontaneous emulsification, which are interesting in themselves, were not studied. The objective was to study experimentally the movement of colloidal species on an out-of-thermal-equilibrium surface, in the system water/glycerol/dodecane/span 80. The interface appears as a convex meniscus when putting water/glycerol on oil with the added non-ionic surfactant in a stainless steel cell composed of two concentric cylindrical holes. Due to the surfactant characteristics, we observed water/glycerol droplets in dodecane, which are generated spontaneously and constitute the colloidal species. The emulsification process happens at the interface, which in the observation region is considered as a plane, because the meniscus curvature's radius is much larger than the droplets displacement analysed. The presence of glycerol slows down the droplets movement, allowing the observation of trajectories of longer time than those obtained without glycerol. The droplets move towards the lowest point of the meniscus and form a crystal-like colloidal structure. We analyse the last stage formation, when only few droplets are produced. The water droplets move attached to the interface while still growing from submicron sizes to a few microns. Although the dynamic nature of the process, with both the interface and colloidal species continuously changing and producing heterogeneities in the system, anomalous diffusion was not observed. The motion of the droplets has a well-identified Brownian component with a Gaussian distribution of

positions due to the thermal agitation of the media surrounding the droplets and a drift component due to the effect of gravity. In addition, temporal changes in droplet behaviour were observed, such as a decrease in the number of droplets moving towards the crystal structure and a decrease in their velocity.

On the other hand, to qualitatively evaluate the encapsulation capacity in spontaneous emulsification, experiments were carried out in a horizontal glass cell with the immiscible liquids on the same observation plane. The interface was approximately flat, in the aqueous phase the species to be evaluated were added: fluorescent molecules (dextran-rhodamine and dextran-fluorescein), $CdSe/ZnS$ nanocrystals and colloidal nano-particles. While in the oily phase, span 80 was added. In this configuration, droplets formed by spontaneous emulsification move away from the interface by simple diffusion, some of them contained the test species, so it was possible to evaluate whether or not the test species crossed the interface. In the case of fluorescent molecules, all formed droplets were observed to contain the test species, whereas in the case of $CdSe/ZnS$ nanocrystals and colloidal nano-particles, the self-assembly of the test species at the interface made encapsulation less efficient, which was achieved only in a few droplets and after several days of observation. Due to the dynamic nature of the interface and the colloidal self-assembly, it was also found that the droplets formed a wide variety of structures.

ACKNOWLEDGMENTS

I imagined myself many times writing the acknowledgments of the thesis. Now that it's finally over, I don't know what to say because I feel like I've already said everything. To start writing I remember my first day at the Physics Institute and how things have changed since then. I suddenly remember, what I want to say.

Thanks to my thesis advisor, Dr. José Luis Arauz, for all his teachings on this long journey of 6 years. Also thanks to Dr. Rosario Moctezuma and Dr. Rodrigo Vélez for their support. My eternal gratitude to the people who have formed and are part of the LFC, my days would not have been the same without you.

Of course I appreciate the support of the PCI program staff and to CONACYT for the scholarship granted that allowed me to continue with my studies.

Thanks to my family for all their love and support, especially my parents María and Jesús, thanks for everything. I love you. Thanks to the people I've known for years and are still my friends, thanks for giving me your time and sharing pleasant moments.

Special thanks to this beautiful state: San Luis Potosí, where I met incredible people, visited beautiful places, met my favorite writer, and spent hours in its museums and in the Cineteca *Alameda*.

CONTENTS

Part I

THESIS

INTRODUCTION

For some persons, doing research in physics is an art, where the beauty lies in the methodological process from natural phenomena to models. Since ancient times, it starts with the observation of natural phenomenon. Then, according with the scientific method, it follows a qualitative idea on *How one can interpret the phenomenon*, and then one proceeds with the construction of a model with the aim to reproduce as good as possible the observed phenomenon. This is precisely what we did, the observation of the movement of droplets generated by spontaneous emulsification on an interface. Such movement was described by proposing a simple model.

In the literature there are several publications that study the motion of colloidal particles, with the objective of creating the methods of an efficient control of mass and charge transport through deep understanding of the diffusion mechanisms of micro or nano objects. A topic of interest and about which many questions remain is the motion in out of thermal equilibrium systems. Our study system is relevant in this aspect, since we have water/glycerol droplets generated by spontaneous emulsification that move over an interface between water/glycerol/oil/span 80. In addition, the droplets remain attached to the interface, since it is observed that they continue to grow as a function of time. Spontaneous emulsification is not a thermodynamic equilibrium process but instead is highly dependent on initial conditions such as the initial composition of the oil and water phases, and we study the droplets movement on the interface.

We had many questions related to the subject of how do the droplets move and the medium in which they were found. Being an out-of-equilibrium system, does the droplets movement present anomalous diffusion? The answers were found in the analysis of individual trajectories, in which it was assumed that the movement was ergodic, i.e., all the steps were identically distributed and that taking the time average was equivalent to taking the average over the ensemble. The work of this thesis is to contribute to understand the motion of colloidal particles in systems out of the thermal equilibrium. For this, a way to satisfactorily describe the movement at the interface water/oil

of droplets generated by spontaneous emulsification was developed.

The thesis consists of six chapters including the present one and appendixes. In chapter two, the theoretical concepts about Brownian motion and diffusion are exposed, while in chapter three the background of the topics of interest in the development of the thesis is presented, mainly those related to spontaneous emulsification. In chapter four and five, the results are presented, which are divided in three general groups: those related to the movement of the droplets, those referring to the crystalline structure (CS) and those related to the encapsulation capacity and self-assembly in spontaneous emulsification. Finally, in chapter six, the conclusions of the work and possible future work options are presented. Regarding the appendices A and B, they include original work about experimental details and complementary experimental results. Appendix A includes information related to the experimental set up and the conditions developed to propose the analyses. In the appendix B, complementary results to chapter four and five are presented. Finally, in Appendix C are included the permissions of use for the images included in chapters three and four.

UBIQUITY OF DIFFUSION IN SOFT MATTER

Let us start by recalling the simple experiment that many people have done once, where a drop of dye is placed in a bowl of liquid. Here we can observe the change in the dye's concentration by diffusion, which is the important transport process occurring in many phenomena in science and technology. In living organisms, diffusion is a major transport mechanism. For example, in the cerebellum the propagation of molecular signalling for metabolism and synaptic plasticity (both intra-cellularly and extra-cellularly) is done by diffusion [1] or the random walk performed by the bacteria E. coli while they alternate between purposeful swimming and tumbling [2]. Moreover, diffusion often controls self-assembly [3], [4] which is fundamental in the fabrication of different devices that include the functionality of molecular components [5].

In this chapter the Brownian motion is discussed and the simplest physical quantity used for its description: the mean square displacement (MSD). According with the time dependence of the MSD there are two kinds of diffusion in unbounded systems: normal and anomalous. There are other special cases, for example confined motion, Brownian motion with drift and, due to the relevance to soft matter, at aqueous interfaces. They are topics of special interest in this thesis work because they give the mathematical framework for the analysis of our system.

2.1 BROWNIAN MOTION

Colloidal particles are constantly in motion due to the solvent thermal fluctuations. To have an idea, there are about 10^{21} collisions per second of the molecules in the medium with the Brownian particle [6]. This phenomenon is referred as Brownian motion, in honour to the English botanist Robert Brown, who in 1828 observed the irregular motion of small pollen grains in water [7]. However, the first person who observed this irregular movement, but in charcoal particles, was Jan Ingen-Housz 43 years before in 1784 [8].

The quantitative explanation of the Brownian motion came independently from Albert Einstein (1905) and Marian Smoluchowski (1906)

[9]. Einstein was able to determine the mean square displacement of a Brownian motion in terms of the Avogadro's number, so that he linked diffusion with statistical mechanics and indirectly confirmed the existence of molecules and atoms. Some years later, in 1926 Jean Perrin won the physics Nobel Prize for experimentally verifying Einstein's work [10].

The diffusion equation for Brownian particles in a solvent without interactions and external potentials (eq. 2.1) was obtained for Albert Einstein, taking as starting point the heat kinetic-molecular theory.

$$\frac{\partial n(\vec{\mathbf{r}}, t)}{\partial t} = D \nabla^2 n(\vec{\mathbf{r}}, t), \tag{2.1}$$

where $n(\vec{\mathbf{r}}, t)$ is the particle concentration at the position $\vec{\mathbf{r}}$ at time t, and D is the diffusion coefficient for not interacting Brownian particles (i.e., in the limit of dilute systems). For spherical particles of radius R, D is given by the Stokes-Einstein equation:

$$D = \frac{k_B T}{6 \pi \eta R}, \tag{2.2}$$

where k_B is the Boltzmann's constant, T is the absolute temperature and η is the viscosity of the medium.

2.2 MEAN SQUARE DISPLACEMENT

The simplest quantity describing Brownian motion is the mean square displacement, $W(t) \equiv \langle [\vec{\mathbf{r}}(t) - \vec{\mathbf{r}}(0)]^2 \rangle / (2dim)$, where $\vec{\mathbf{r}}(t)$ is the particle position at time t and dim is the system's dimension [11]. The angle brackets indicate average over an equilibrium ensemble. For isotropic systems, the motion along coordinate axes are statistically independent. Thus, $W(t)$ can be described in terms of the particle's displacements along one direction, for instance, x, as follows:

$$W(t) = \langle [x(t) - x(0)]^2 \rangle / (2), \tag{2.3}$$

In the limit of infinite dilution, i.e. for non-interacting particles in a $3D$ homogeneous suspension, $W(t)$ is a linear function of time, $W(t) = D_0 t$ [12]. Besides, in the literature we can find analytical expressions for different kinds of motion [13], [14]. For simplicity, in one direction and as an example (fig. 2.1), we have:

$$\langle [x(t) - x(0)]^2 \rangle = \begin{cases} 2Dt \; normal \; diffusion \\ 2Dt + (vt)^2 \; Brownian \; motion \; with \; drift \\ \frac{L_m^2}{3} \left[1 - exp \left(\frac{-t}{\tau_m} \right) \right] \; Confined \; motion \\ 2D_\alpha t^\alpha \; anomalous \; diffusion \end{cases} \quad (2.4)$$
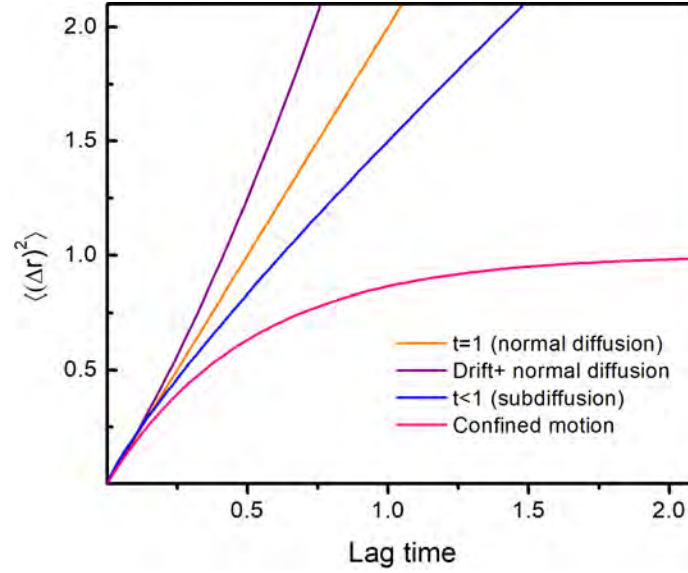
Figure 2.1: Mean square displacement as a function of time for different kind of motion.

where v is the drift velocity, L_m is the measured (or apparent) domain size, τ_m is the equilibration time and D_α is the generalized diffusion constant with dimensions cm^2/s^α. Furthermore, according with the exponent α in the power law-form relating the Mean Square Displacement and time, eq. 2.5, one can recognize two types of diffusion: normal and anomalous.

$$\langle \Delta x^2(t) \rangle = D_\alpha t^\alpha, \quad (2.5)$$

If $\alpha = 1$, the diffusion is normal. In the other case, ($\alpha \neq 1$) the diffusion is anomalous. There are two special cases of anomalous diffusion: subdiffusion ($0 < \alpha < 1$) and superdiffusion ($\alpha > 1$) [15]. In the following paragraphs, will be described them in more detail.

2.3 NORMAL DIFFUSION

Diffusion is an important mechanism for transport in different environments. Just to mention some cases: 1) for solutes (e.g. oxygen, nitrous oxide and carbon dioxide) in biofilms [16]; 2) for small molecules through polymer solutions near the glass transition point [17]; 3) for radionuclides through engineered containment barriers [18]; 4) for contaminants (e.g. sand, bentonite, cadmium) in water [19].

There are mainly two approaches from which normal diffusion is studied: a macroscopic aspect with Fick's law and a microscopic aspect with Einstein's Formalism [20]. Here we will work with this second approach. The conditions assumed by Einstein in his derivation of the diffusion equation (eq. 2.1) are:

- The independence of the individual particles.

- There is a minimum time scale below which individual displacements become statistically independent from each other.

- During the mentioned time scale, the particle displacements are symmetrically distributed around a typical mean free path in both positive and negative directions.

The previous mention ideas of Normal diffusion are usually considered in systems that are in or very close to thermal equilibrium [21].

2.3.1 *Probability distribution functions*

Brownian motion is a stochastic process which can be described in fundamental form by the transition probability distribution function $P(\Delta \vec{r}, t)$ of particle displacements $\Delta \vec{r} = \vec{r}(t) - \vec{r}(0)$ during a time t. The important characteristics of this functions, resume as follows [22]:

- The transition probability is normalized, i.e. $\int P(\Delta \vec{r}, t) d\vec{r} = 1$

- The orthogonal directions, for example x, y in a two dimensional system, are independent. Therefore, $P(\Delta \vec{r}, t) = P(\Delta x, t) P(\Delta y, t)$, where $P(\Delta x, t)$ and $P(\Delta y, t)$ are the probability functions in the directions x, y respectively at time t.

- The expected value for any function $f(\Delta \vec{r})$ is,

$$\langle f(\Delta \vec{r}) \rangle = \int f(\Delta \vec{r}) P(\Delta \vec{r}, t) d\vec{r}, \tag{2.6}$$

$\langle \Delta x^m \rangle \equiv \mu_m$ is the m-th moment of $P(\Delta x, t)$, and μ_1 is the mean value. For equilibrium systems $\mu_1 = 0$, because the Brownian particle can move in any direction with the same probability. The second moment is $2W(t)$.

- In a isotropic system made up of non interacting particles, the probability distribution functions are Gaussian functions centered at $\Delta x = 0$, i.e., $\langle \Delta x \rangle = 0$ and variance $\sigma(t) \equiv \sqrt{\langle \Delta x^2(t) \rangle} = \sqrt{2Dt}$ [23]. So that, we can built the normalize Gaussian functions:

$$P_G(\Delta x, t) = \frac{1}{\sqrt{4\pi Dt}} exp \left[-\frac{\Delta x^2}{4Dt} \right], \tag{2.7}$$

2.4 ANOMALOUS DIFFUSION

In anomalous diffusion process, at least one of the fundamental assumptions mentioned in last section 2.3 is broken and the strong convergence to the Gaussian, according to the central limit theorem, is not fulfilled [24]. Anomalous diffusion can be found in complex environments, such as 1)Biological systems: for example diffusion of fluorescently labelled mRNA [25], endogenous lipid granules [26] in the cytoplasm of living cells; lateral diffusion of transferrin receptor [27], phospholipids and cholesterols [28] in membranes. 2)Caging of some sort: for example a particle pulled by a constant force in a glass-forming Yukawa mixture [29]. 3)Inhomogeneous media: for example, colloidal tracer particles in entangled F-actin networks [30]. 4)Porous media for example, diffusion of tracer particles in porous samples made of packings of activated carbon porous grains [31]. The above systems are examples where subdiffusion has been observed. On the other hand, superdiffusion has been reported in the motion of organic largish molecules on the $Cu(110)$ surface [32] and atomic clusters of gold $Au140$ adsorbed on graphite [33].

Immediately the question of how to model such phenomena arises. In the literature different models (that depend on the characteristics of the medium in which the anomalous diffusion occurs) can be found such as the following [34]: 1)Continues time Random walk formalism (CTRW), where the consideration is that the particle waits random time intervals between jumps of different length. 2)Fractional Brownian motion (fBm) is a continuous time Gaussian process, where the steps are not necessarily independent. 3)Another Gaussian process

but with a Time-dependent diffusion coefficient is the Scaled Brownian motion (SBM). 4)In crowded environments, for example inside of a biological cell, the labyrinthine model is used to mathematically describe the environment. However, this type of model is barely used because most of them don't have an exact solution. An unusual example of exact solution for labyrinthine model is the solution called random walk on a random walk (RWRW).

2.5 DIFFUSION AT INTERFACES

Concerning the work developed in this thesis, it is relevant to mention what is known about diffusion of colloidal particles at interfaces. The behaviour of adsorbed colloidal particles at liquid-liquid interfaces is an important topic for various applications, for example, in micro-rheology, encapsulation, emulsification and the interface-driven assembly.

There are numerous works describing the stability and the interaction of colloids at different two-phases interfaces [35], where different experimental techniques such as optical microscopy, fluorescence correlation spectroscopy, dynamic interfacial tension measurements are used. Just to mention few examples, single-particle tracking was used for Du and coworkers [36] to study 3D nanoparticles (sizes in the range 24 nm to 2000 nm) transport dynamics in a silicone oil-water interface. They found that the difussion coefficient, $D_\parallel$, (2.2) for particles bigger than 200 nm, scales inversely with particles size. In the other hand, interesting aspects arises as the nanoparticle size decreases and approach the length scale of interfacial region: the smaller particles experience greater drag force at the interface, i.e. particles are slower than the predictions of the Stokes-Einstein relation and hydrodynamic theories.

Most of these works try to explain this non-linear dependence between the translational diffusion and the hydrodynamic radius R_H^{-1}, as follows:

- The laminar flow of liquid around the particle is different compared with the Stokes flow, because the presence of the interface introduces an extra boundary condition. Stokes flow is only applicable in interfacial systems consisted of liquids with the same viscosity, such as water and decane [37], and particles with contact angle of 90° [38].
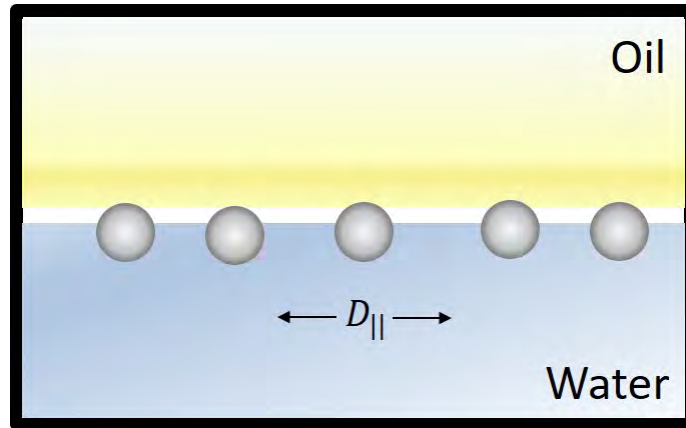
Figure 2.2: Brownian particles at oil-water interfaces and their correspon-
ding diffusion coefficient, $D_\parallel$, parallel to the interface.

- Not only defects on the interface induce multiple metastable pinning of the three phase contact line (particle, oil and water) but also the particle size changing contact angle Θ. Thermally activated deformations of the interface at the triple line drive the system out of mechanical equilibrium producing an extra reverse random force associated with extra viscous drag and as a result, diffusion slows [39].

- Using a generalized Stokes-Einstein relation, it's possible approximate $D_\parallel$ considering the particle cross-sectional area immersed in the respective fluid phases.

$$D_{SE\parallel} = 2\pi k_B T / (6\pi R_H (2\pi \eta_w + (\eta_a - \eta_w)(2\Theta - sen2\Theta))), \quad (2.8)$$

Where η_a and η_w are the viscosity of the phases, for example alkane (oil) and water, respectively [40].

In addition, other particle shapes experiment a drag at the interface larger than in the bulk, such as polystyrene ellipsoids of different aspect ratios trapped at the air-water interface [41].

REFERENCES

[1] T. M. Marinov and F. Santamaria, "Chapter Eight - Computational Modeling of Diffusion in the Cerebellum," in *Computational Neuroscience*, ser. Progress in Molecular Biology and Translational Science, K. T. Blackwell, Ed., vol. 123, Academic Press, 2014, pp. 169–189 (cit. on p. 4).

[2] H. Huo, R. He, R. Zhang, and J. Yuan, "Swimming Escherichia coli cells explore the environment by Lévy walk," *Applied and Environmental Microbiology*, vol. 87, no. 6, e02429–20, 2021 (cit. on p. 4).

[3] J. Y. Chung, A. J. Nolte, and C. M. Stafford, "Diffusion-controlled, self-organized growth of symmetric wrinkling patterns," *Advanced Materials*, vol. 21, no. 13, pp. 1358–1362, 2009 (cit. on p. 4).

[4] M. Ozmaian, A. Fathizadeh, M. Jalalvand, M. R. Ejtehadi, and S Allaei, "Diffusion and self-assembly of C60 molecules on monolayer graphyne sheets," *Scientific Reports*, vol. 6, no. 1, pp. 1–10, 2016 (cit. on p. 4).

[5] J. V. Barth, "Molecular architectonic on metal surfaces," *Annual Review of Physical Chemistry*, vol. 58, pp. 375–407, 2007 (cit. on p. 4).

[6] S. Chandrasekhar, "Stochastic problems in physics and astronomy," *Reviews of Modern Physics*, vol. 15, no. 1, p. 1, 1943 (cit. on p. 4).

[7] R. Brown, "XXIV. Additional remarks on active molecules," *The Philosophical Magazine*, vol. 6, no. 33, pp. 161–166, 1829 (cit. on p. 4).

[8] P. W. Van der Pas, "The discovery of the Brownian motion," *Scientiarum Historia*, vol. 13, no. 1, pp. 27–35, 1971 (cit. on p. 4).

[9] P. Hänggi and F. Marchesoni, "Introduction: 100 years of Brownian motion," *Chaos: An Interdisciplinary Journal of Nonlinear Science*, vol. 15, no. 2, p. 026 101, 2005 (cit. on p. 5).

[10] C. Bigg, "Evident atoms: Visuality in Jean Perrin's Brownian motion research," *Studies in History and Philosophy of Science Part A*, vol. 39, no. 3, pp. 312–322, 2008 (cit. on p. 5).

[11] J. L. Arauz-Lara, "Colloidal Fluids," in *Fluids, Colloids and Soft Materials*. John Wiley & Sons, Ltd, 2016, ch. 11, pp. 187–201, ISBN: 9781119220510 (cit. on p. 5).

[12] M. Carbajal-Tinoco, G. C. de León, and J. Arauz-Lara, "Brownian motion in quasibidimensional colloidal suspensions," *Physical Review E*, vol. 56, no. 6, p. 6962, 1997 (cit. on p. 5).

[13] M. J. Saxton and K. Jacobson, "Single-particle tracking: Applications to membrane dynamics," *Annual Review of Biophysics and Biomolecular Structure*, vol. 26, no. 1, pp. 373–399, 1997 (cit. on p. 5).

[14]   N. Destainville and L. Salomé, "Quantification and correction of systematic errors due to detector time-averaging in single-molecule tracking experiments," *Biophysical Journal*, vol. 90, no. 2, pp. L17–L19, 2006 (cit. on p. 5).

[15]   J. Klafter, A. Blumen, and M. F. Shlesinger, "Stochastic pathway to anomalous diffusion," *Physical Review A*, vol. 35, no. 7, p. 3081, 1987 (cit. on p. 6).

[16]   P. S. Stewart, "Diffusion in biofilms," *Journal of Bacteriology*, vol. 185, no. 5, pp. 1485–1491, 2003 (cit. on p. 7).

[17]   O. Karlsson, J. Stubbs, L. Karlsson, and D. Sundberg, "Estimating diffusion coefficients for small molecules in polymers and polymer solutions," *Polymer*, vol. 42, no. 11, pp. 4915–4923, 2001 (cit. on p. 7).

[18]   C. D. Shackelford and S. M. Moore, "Fickian diffusion of radionuclides for engineered containment barriers: Diffusion coefficients, porosities, and complicating issues," *Engineering Geology*, vol. 152, no. 1, pp. 133–147, 2013 (cit. on p. 7).

[19]   C. D. Shackelford, "Laboratory diffusion testing for waste disposal: A review," *Journal of Contaminant Hydrology*, vol. 7, no. 3, pp. 177–217, 1991 (cit. on p. 7).

[20]   A. Einstein, *Investigations on the Theory of the Brownian Movement*. Courier Corporation, 1956 (cit. on p. 7).

[21]   G. Parisi, "Brownian motion," *Nature*, vol. 433, no. 7023, pp. 221–221, 2005 (cit. on p. 7).

[22]   M. Carbajal-Tinoco, "Propiedades estructurales de suspensiones coloidales confinadas," Ph.D. dissertation, Universidad Autónoma de San Luis Potosí, 1997 (cit. on p. 7).

[23]   D. A. McQuarrie, *Statistical Mechanics*. Harper & Row, 1973, pp. 452–460 (cit. on p. 8).

[24]   J.-P. Bouchaud and A. Georges, "Anomalous diffusion in disordered media: Statistical mechanisms, models and physical applications," *Physics Reports*, vol. 195, no. 4-5, pp. 131–140, 1990 (cit. on p. 8).

[25]   I. Golding and E. C. Cox, "Physical nature of bacterial cytoplasm," *Physical Review Letters*, vol. 96, no. 9, p. 098 102, 2006 (cit. on p. 8).

[26]   J.-H. Jeon, V. Tejedor, S. Burov, *et al.*, "In vivo anomalous diffusion and weak ergodicity breaking of lipid granules," *Physical Review Letters*, vol. 106, no. 4, p. 048 103, 2011 (cit. on p. 8).

[27]   K. Ritchie, X.-Y. Shan, J. Kondo, K. Iwasawa, T. Fujiwara, and A. Kusumi, "Detection of non-Brownian diffusion in the cell membrane in Single Molecule Tracking," *Biophysical Journal*, vol. 88, no. 3, pp. 2266–2277, 2005 (cit. on pp. 8, 27).

[28]   J.-H. Jeon, H. M.-S. Monne, M. Javanainen, and R. Metzler, "Anomalous diffusion of phospholipids and cholesterols in a lipid bilayer and its origins," *Physical Review Letters*, vol. 109, no. 18, p. 188 103, 2012 (cit. on pp. 8, 27).

[29]   D Winter, J Horbach, P Virnau, and K Binder, "Active nonlinear microrheology in a glass-forming Yukawa fluid," *Physical Review Letters*, vol. 108, no. 2, p. 028 303, 2012 (cit. on pp. 8, 27).

[30]   I. Wong, M. Gardel, D. Reichman, *et al.*, "Anomalous diffusion probes microstructure dynamics of entangled F-actin networks," *Physical Review Letters*, vol. 92, no. 17, p. 178 101, 2004 (cit. on pp. 8, 27).

[31]   G. Drazer and D. H. Zanette, "Experimental evidence of power-law trapping-time distributions in porous media," *Physical Review E*, vol. 60, no. 5, p. 5858, 1999 (cit. on p. 8).

[32]   M Schunack, T. R. Linderoth, F Rosei, E. Lægsgaard, I. Stensgaard, and F. Besenbacher, "Long jumps in the surface diffusion of large molecules," *Physical Review Letters*, vol. 88, no. 15, p. 156 102, 2002 (cit. on p. 8).

[33]   W. Luedtke and U. Landman, "Slip diffusion and Lévy flights of an adsorbed gold nanocluster," *Physical Review Letters*, vol. 82, no. 19, p. 3835, 1999 (cit. on p. 8).

[34]   I. M. Sokolov, "Models of anomalous diffusion in crowded environments," *Soft Matter*, vol. 8, no. 35, pp. 9043–9052, 2012 (cit. on p. 8).

[35]   B. P. Binks, "Particles as surfactants: Similarities and differences," *Current Opinion in Colloid & Interface Science*, vol. 7, no. 1-2, pp. 21–41, 2002 (cit. on pp. 9, 31).

[36]   K. Du, J. A. Liddle, and A. J. Berglund, "Three-dimensional real-time tracking of nanoparticles at an oil–water interface," *Langmuir*, vol. 28, no. 25, pp. 9181–9188, 2012 (cit. on p. 9).

[37]   A. Nelson, D. Wang, K. Koynov, and L. Isa, "A multiscale approach to the adsorption of core–shell nanoparticles at fluid interfaces," *Soft Matter*, vol. 11, no. 1, pp. 118–129, 2015 (cit. on p. 9).

[38] D. Wang, S. Yordanov, H. M. Paroor, *et al.*, "Probing diffusion of single nanoparticles at water–oil interfaces," *Small*, vol. 7, no. 24, pp. 3502–3507, 2011 (cit. on p. 9).

[39] G. Boniello, C. Blanc, D. Fedorenko, *et al.*, "Brownian diffusion of a partially wetted colloid," *Nature Materials*, vol. 14, no. 9, pp. 908–911, 2015 (cit. on pp. 10, 44).

[40] D. Wang, Y.-L. Zhu, Y. Zhao, *et al.*, "Brownian diffusion of individual Janus nanoparticles at water/oil interfaces," *ACS nano*, vol. 14, no. 8, pp. 10 095–10 103, 2020 (cit. on p. 10).

[41] G. Boniello, A. Stocco, M. Gross, M. In, C. Blanc, and M. Nobili, "Translational viscous drags of an ellipsoid straddling an interface between two fluids," *Physical Review E*, vol. 94, no. 1, p. 012 602, 2016 (cit. on p. 10).

INTERFACIAL PHENOMENA: SPONTANEOUS EMULSIFICATION AND COLLOIDAL SELF-ASSEMBLY

Emulsions are colloidal dispersions of two immiscible liquids called discontinuous and continuous phase, i.e., droplets and the environment that surrounds them, respectively. As is sketched in fig. 3.1, the system is stabilized by a surfactant, whose function is to decrease the interfacial tension and as consequence to decrease the free energy, G, for droplets formation [42].
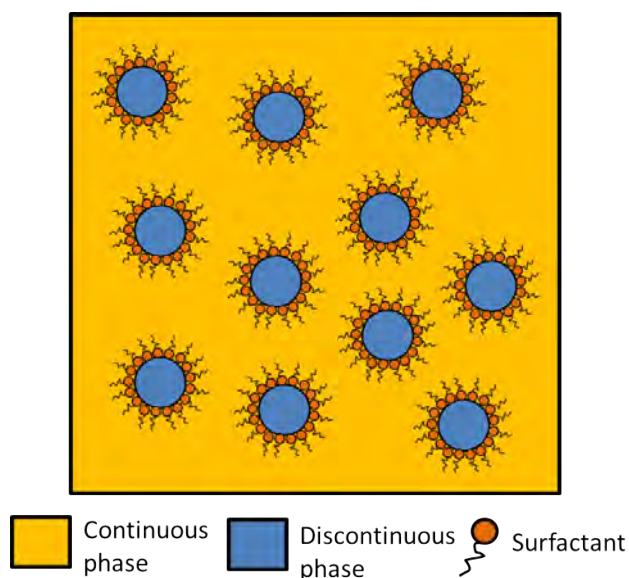

Figure 3.1: Emulsions are formed by droplets (discontinous phase), suspended in a medium (continous phase) and stabilized by a surfactant.

Normally, to make emulsions it is necessary supply energy to the system, $\Delta G > 0$, e.g., mechanical, thermal, or ultrasound. This energy allows one phase (the discontinuous phase) to be dispersed in the continuous phase, increasing the interfacial area. In practice, the energy necessary for forming and shrinking droplets, is greater than the theoretically calculated because the viscous resistance of the emulsion phases must be overcome [43]. On the other hand, if the two immiscible liquids are not in equilibrium, gradients in chemical potential between phases can generate negative free energy values, $\Delta G < 0$, and the emulsification occurs spontaneously, i.e., emulsions are pro-

duced without the supply of external energy to the system [44].

Although the subject of this thesis is not to explain the spontaneous emulsification phenomenology in the studied system, a review of the existing literature on the topic is presented. In addition, a brief description of self-assembly at interfaces is presented. Likewise, the works carried out in the Complex Fluids Laboratory on spontaneous emulsification are also mentioned, which are the direct antecedents of this thesis.

3.1 MECHANISMS OF SPONTANEOUS EMULSIFICATION

Since 1878, when Johannes Gad first observed the phenomenon of spontaneous emulsification (SE) [45], numerous systems where it occurs and possible applications have been reported. However, the phenomenon of SE is still not fully understood. The mechanisms proposed in the literature to explain SE can be summarized as interfacial turbulence, negative interfacial tensions, diffusion and stranding, swelling micelles, Rayleigh-Plateau instability and Marangoni flow. It may even be that it is not a single mechanism but several mechanisms acting at the same time. All of them are briefly described below.

- Interfacial turbulence: This mechanism was originally proposed by Quincke in 1888 for describing the SE in solutions of lauric acid in oil in contact with aqueous sodium hydroxide. Quincke described the SE as a result of localized interfacial tension lowering, due to the non-uniform soap formation at different points in the interface. The subsequent turbulence (and hence the name) may tear droplets of oil away from the interface, which are then stabilized by the soap produced [45].

- Negative interfacial tensions: When the interfacial tension is locally negative, the interface area tends to increase spontaneously, forming emulsion droplets. The increase of interfacial area allows the interfacial tension to become less negative. An example where this mechanism is proposed as an explanation to SE was put forward for Granek, Ball and Cates [46]. They gave a mathematical description for SE in the system oleic acid/oil/aqueous alkali, using Free energy model including surfactant transport.

- Difussion and stranding: In this case the relative solubility of each phase in the other, plays a fundamental role. For example, in a solution of ethyl alcohol and toluene in contact with water, the alcohol diffuses from the oil into de water, carrying with it

some oil. As the alcohol diffuses further into the water, the associated oil becomes thrown out of solution, and is *stranded* in the water forming emulsion droplets. The inverse case, an emulsion of water in oil formed in the oil interface side, is also possible as the ethyl alcohol diffuses from the aqueous phase into the oil carrying some water, the water becomes *stranded* in the oil. Ruschak and Miller proposed the *diffusion path* theory [47], which offers a mathematical explanation of the formation of areas with local oversaturation. When solving diffusion equations for ternary systems with semi-infinite immiscible phases, it was found that, subject to specific conditions, the composition of the system remains constant over time and can be plotted directly on the ternary phase diagram.

- Swollen micelles: Spontaneous emulsification can be driven by the solubilization of molecules of one phase in another within the micelles formed by the surfactant, hence the term swollen micelles. Usually, SE is associated with ultra-low surface tensions however, there are cases where this is not the rule. For example, in the system of water droplet surrounded by kerosene and span 80, reported by Silva and co-workers [48] where the interfacial tension was not lower than $4\,mN/m$, but the surfactant concentration was above Critical Micelle Concentration (CMC). They observed SE, as time passed the organic phase becomes cloudy due the increase of the number of water droplets (with size $\approx 200\,nm$) in the oil phase and the volume of the water droplet decreased.

- Rayleigh-Plateau instability: Droplets can form due to the existence of small disturbances in a liquid stream. This is explained if the perturbations break down into sinusoidal components, with the rate of grow or decrease being related to the wave number and the initial stream radius [49]. The mechanism has been proposed to explain spontaneous emulsification, in systems with in-situ surfactants. As described by Ballard and co-workers [50] in the system Water/KOH/Oleic acid/Styrene/Stearyl acrylate. The neutralization reaction between KOH and Oleic acid, by which potassium oleate is formed, creates a very dense interfacial layer that destabilizes the interface. Interface deformation causes Rayleigh-Plateau instability that results in the formation of new daughter droplets that can continue to subdivide until the concentration of oleic acid within the droplet is consumed.

- Marangoni flow: Huang and co-workers [51] explains how Marangoni flow can cause SE. They use Poly(ethylene oxide)(PEO) star polymers, these have characteristics of both colloidal particles and soluble polymers and they are considered as very efficient emulsifying agents. Analysing its interfacial activity, it was observed that when PEO was dispersed in xylene and this mixture was placed in contact with water, the phenomenon of spontaneous emulsification occurred. To explain how it happens, it is proposed a hypothetically mechanism of action in which the two liquids are not initially in equilibrium, since there is a force that distributes the PEO in both phases. In a first stage, the PEO is in the xylene phase, but when it comes into contact with water, part of the PEO is adsorbed at the interface, while another part begins to diffuse in the aqueous phase because the polymer is more soluble in this phase. The adsorption of PEO reduces the interfacial tension and increases the interface fluctuations. This local non-uniformity leads to a Marangoni flow that causes droplet formation. Interfacial shear can help separate droplets from the interface, leading to spontaneous emulsification.

3.1.1 *Applications*

SE is an interesting and surprising phenomenon, not only because systems behaviour in which it has been observed, but also the applications of the phenomenon itself. We can mention, for example, that SE can be used to improve some experimental techniques, such as protein crystallization. In the traditional way, protein crystallization is made using the nucleation method. The main inconvenients of this method are the relative long time and small volume required. For this reason, Fukuyama and co-workers [52] proposed a simpler system to control the rate of water transport, based on nano-droplet formation by SE. Micro-droplet containing the protein and precipitant is exposed to an organic phase containing Span 80 as surfactant and nano-droplets form spontaneously at the micro-droplet interface. During the process of forming nano-droplets, water is transferred from the micro-droplet to the nano-sized ones, while the protein and precipitant are retained in the micro-droplet. This leads to an increase in the concentration of protein and precipitant, ultimately resulting in the formation of a crystal of protein. Other important SE application for improve an experimental technique is in the synthesis of Poly(lactic-co-glycolic acid) (PLGA) nanoparticles [53]. One of the most widely used technique for preparing PLGA nanoparticles is emulsification diffusion (ESD), but especially modified SE solvent diffusion (modified-SESD) presents

better properties such as high percentage of drug entrapment and narrow size distribution [54]. In particular, Chen and co-workers [53] exploited modified-SESD for synthesize PLGA-Curcumine nanoparticles taking into account diffe- rent parameters, such as volume ratio of organic solvents, the concentration of surfactant, the percentage of yield, the drug loading and the encapsulation content. In addition, Weerapol and co-workers [55] used SE as drug delivery system for improve the dissolution and oral bioavailability of nifedipine (NDP).

On the other hand, Kowacz and co-workers [56] reported SE in the ionic liquid/aqueous solution of an inorganic salt (IL/W) interface. They observed the formation of nano-sized emulsions without the need to add surfactant. The emulsion droplets are employed to create core shell micro-crystals with potential functionality. Particularly the $[C12mim][NTf2]/Na_2CO_3$ system was used to form fluorescent vaterite ($CaCO_3$) micro-crystals with hollow cores and permeable walls. These microparticles can find applications as carrier and delivery systems enabling pH-controlled target release. Another important potential application of SE is oil recovery because the O/W emulsion have low viscosity and good migration behaviour than oil flow alone [57]. Other advantage is that immiscible oil and water can form an emulsion only relying on the action of emulsifier itself and no external work is needed. An example of this application was reported by Jiang and co-workers [58]. They used fatty acid alkanolamide bipolyoxyethylene ether (NS) for emulsify spontaneously the heavy oil.

Probably the most extended application for SE is in the food science [59] as a low energy method for emulsifying. There are many articles about nano-emulsions via SE using different essential oils, such as citrus oils [60], peppermint oil [61], limonene oil [62], etc. A recent application of SE is reported by Nagasaka and coworkers [63]. They construct a model system that spontaneously produces amino acid-based surfactants at room temperature by the reaction between the organic solvent (octanal) and amino acid (histidine). They observed that the produced surfactant destabilizes the interface causing SE. In addition, when the organic solvent is placed on an aqueous phase as a droplet, the droplet is self-propelled and experiments fusion and division due the chemical Marangoni effect caused by the synthesized surfactants. For that, Nagasaka and co-workers considered the system as a model of primitive cellular metabolism. One more application of SE in biology is surfactant sculpting of biologically inspired hierarchical surfaces [64].

Finally, there are also systems in which spontaneous emulsification is not desired, as for example that produced in the ocular cavity after injection of intraocular tamponade agents based on silicone oils to repair the detachment of retina [65].

3.2 COLLOIDAL SELF-ASSEMBLY AT INTERFACES

There are several methods to obtain ordered two-dimensional structures, for example, spin coating [66], dip coating [67] and electrophoretic deposition [68]. Self-assembly of particles at fluid interfaces has also been used to form colloidal crystals, in which the effects of sedimentation, vertical deposition, physical confinement, electric and magnetic field have been studied [69].

Colloids at fluid interfaces play an important role in the production of various types of two-dimensional structures due the interparticle lateral capillary force between similar particles, which is attractive and produces aggregation and ordering. The range of the capillary forces is usually larger than the Van der Waals forces [70]. Particle bonding at the interface boundary is often accompanied by interfacial deformation near the particle. This deformation give rise to lateral capillary interaction between the particles. The greater the interfacial deformation created by the particles, the stronger the interaction between them. The attraction appears because the liquid meniscus deforms in such a way that the gravitational potential energy of the two particles decreases when they get closer to each other [71].

Of particular interest for this work are colloidal crystal structures at curved interfaces. Examples of curved crystals are colleidosomes, viral capsids, ordered arrangements of copolymers and vesicles, their study is interesting because the curved crystal order affects the mechanical properties of these structures [72]. In a flattered colloidal crystal, each particle in the lattice has six nearest neighbours arranged in a hexagon such that each component triangle of it subtends an angle of $\pi/3$. However, on a curved surface, long-range crystal order and Gaussian curvature are discordant and so a perfect two-dimensional colloidal crystal cannot exist on a curved surface. For example, it has been shown that the lowest energy state of a colloidal crystal on a sphere surface is a configuration in which each 5-sided topological disclination is accompanied by a line of dislocations (pairs of five and seven fold disclinations). This grain boundary, known as *defect scar*, has finite length which is related linearly with the sphere's radius [73]. Defect scars on curved colloidal crystals can be use as a model to

understand the structural defects in solids [74], as functional sites in inorganic or biological systems for chemical reactions and as starting points for bacterial cell division [75].
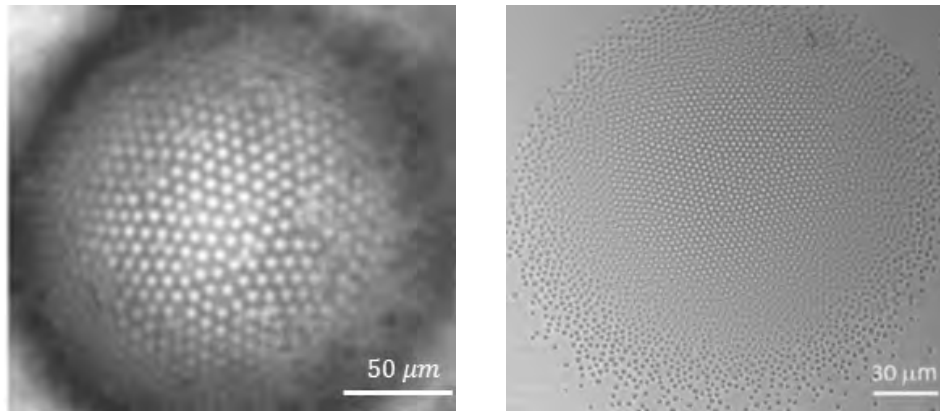
(a) SE on curved interface. Adapted with permission from [76]. Copyright 2007, American Chemical Society.

(b) Crystal structure produced during SE. Adapted with permission from [77]. Copyright 2012, Elsevier.

Figure 3.2: Spontaneous emulsification has been studied in our research group, evaluating the evolution of the droplets over time from their final position in the crystalline structure.

3.3 SPONTANEOUS EMULSIFICATION IN PREVIOUS WORKS IN OUR LAB

Previously, our research group has worked with the system water/dodecane/span 80. In this system spontaneous emulsification is observed. The first approach to the phenomenon was from a static point of view. When the three phases were put in contact after gently hand mixing, the spontaneous emulsification of water in oil was observed. On the curved interface between initial water droplets and oil, two-dimensional spherical crystalline colloidal structures were formed as a result of spontaneous emulsification and colloidal self-assembly (figure 3.2a) [76]. In the other hand, in order to improve the control on the interface in these experiments, a stainless steel cell was designed, which is the same as the one used in this thesis work (described in section 4.1). With this arrangement, the crystalline structure formation process was observed (figure 3.2b): once formed, the droplets move (sediment) from the upper to the lower interface part, where they form the mentioned crystalline structure. In addition, it was found that the emulsion droplets radius is a function of time and also that it is related with the surfactant concentration [77].

REFERENCES

[42] L. L. Schramm, *Emulsions, foams, and suspensions: fundamentals and applications*. John Wiley & Sons, 2006 (cit. on p. 15).

[43] B Abismaıl, J. P. Canselier, A. M. Wilhelm, H. Delmas, and C. Gourdon, "Emulsification by ultrasound: Drop size distribution and stability," *Ultrasonics Sonochemistry*, vol. 6, no. 1-2, pp. 75–83, 1999 (cit. on p. 15).

[44] C. Solans, D. Morales, and M. Homs, "Spontaneous emulsification," *Current Opinion in Colloid & Interface Science*, vol. 22, pp. 88–93, 2016 (cit. on p. 16).

[45] J. W. McBain and T.-M. Woo, "Spontaneous emulsification, and reactions overshooting equilibrium," *Proceedings of the Royal Society of London. Series A-Mathematical and Physical Sciences*, vol. 163, no. 913, pp. 182–188, 1937 (cit. on p. 16).

[46] R Granek, R. Ball, and M. Cates, "Dynamics of spontaneous emulsification," *Journal de Physique II*, vol. 3, no. 6, pp. 829–849, 1993 (cit. on p. 16).

[47] K. J. Ruschak and C. A. Miller, "Spontaneous emulsification in ternary systems with mass transfer," *Industrial & Engineering Chemistry Fundamentals*, vol. 11, no. 4, pp. 534–540, 1972 (cit. on p. 17).

[48] P. S. Silva, S. Zhdanov, V. M. Starov, and R. G. Holdich, "Spontaneous emulsification of water in oil at appreciable interfacial tensions," *Colloids and Surfaces A: Physicochemical and Engineering Aspects*, vol. 521, pp. 141–146, 2017 (cit. on p. 17).

[49] S. Aslanov, "Theory of the breakup of a liquid jet into drops," *Technical Physics*, vol. 44, no. 11, pp. 1386–1387, 1999 (cit. on p. 17).

[50] N. Ballard, M. Salsamendi, P. Carretero, and J. M. Asua, "An investigation into the nature and potential of in-situ surfactants for low energy miniemulsification," *Journal of Colloid and Interface Science*, vol. 458, pp. 69–78, 2015 (cit. on p. 17).

[51] Y.-R. Huang, M. Lamson, K. Matyjaszewski, and R. D. Tilton, "Enhanced interfacial activity of multi-arm poly (ethylene oxide) star polymers relative to linear poly (ethylene oxide) at fluid interfaces," *Physical Chemistry Chemical Physics*, vol. 19, no. 35, pp. 23 854–23 868, 2017 (cit. on p. 18).

[52] M. Fukuyama, A. Akiyama, M. Harada, and A. Hibara, "Microfluidic protein crystallisation controlled using spontaneous emulsification," *Analytical Methods*, vol. 7, no. 17, pp. 7128–7131, 2015 (cit. on p. 18).

[53] C. Chen, W. Yang, D.-T. Wang, C.-L. Chen, Q.-Y. Zhuang, and X.-D. Kong, "A modified spontaneous emulsification solvent diffusion method for the preparation of curcumin-loaded PLGA nanoparticles with enhanced in vitro anti-tumor activity," *Frontiers of Materials Science*, vol. 8, no. 4, pp. 332–342, 2014 (cit. on pp. 18, 19).

[54] Z Ye and E Squillante, "The development and scale-up of biodegradable Polymeric Nanoparticles loaded with Ibuprofen," *Colloids and Surfaces A: Physicochemical and Engineering Aspects*, vol. 422, pp. 75–80, 2013 (cit. on p. 19).

[55] Y. Weerapol, S. Limmatvapirat, M. Kumpugdee-Vollrath, and P. Sriamornsak, "Spontaneous emulsification of Nifedipine-loaded self-nanoemulsifying drug delivery system," *An Official Journal of the American Association of Pharmaceutical Scientists*, vol. 16, no. 2, pp. 435–443, 2015 (cit. on p. 19).

[56] M. Kowacz, J. M. Esperança, and L. P. N. Rebelo, "Spontaneous emulsification in ionic liquid/water systems and its use for templating of solids," *Soft Matter*, vol. 10, no. 21, pp. 3798–3805, 2014 (cit. on p. 19).

[57] H. Feng, W. Kang, H. Wu, *et al.*, "Study on the relationship between emulsion stability and droplet dynamics of a spontaneous emulsion for chemical enhanced oil recovery," *Journal of Dispersion Science and Technology*, vol. 39, no. 8, pp. 1214–1222, 2018 (cit. on p. 19).

[58] G. Jiang, D. Tang, and Q. Hu, "Effect of a type of spontaneous emulsification and viscosity reduction agent on the properties of heavy oil," *Petroleum Science and Technology*, vol. 36, no. 11, pp. 781–786, 2018 (cit. on p. 19).

[59] J. S. Komaiko and D. J. McClements, "Formation of food-grade nanoemulsions using low-energy preparation methods: A review of available methods," *Comprehensive Reviews in Food Science and Food Safety*, vol. 15, no. 2, pp. 331–352, 2016 (cit. on p. 19).

[60] S. Zhao, G. Tian, C. Zhao, *et al.*, "The stability of three different citrus oil-in-water emulsions fabricated by spontaneous emulsification," *Food Chemistry*, vol. 269, pp. 577–587, 2018 (cit. on p. 19).

[61] H. Barzegar, M. A. Mehrnia, B. Nasehi, and M. Alipour, "Fabrication of peppermint essential oil nanoemulsions by spontaneous method: Effect of preparing conditions on droplet size," *Flavour and Fragrance Journal*, vol. 33, no. 5, pp. 351–356, 2018 (cit. on p. 19).

[62] A. H. Saberi, Y. Fang, and D. J. McClements, "Influence of surfactant type and thermal cycling on formation and stability of flavor oil emulsions fabricated by spontaneous emulsification," *Food Research International*, vol. 89, pp. 296–301, 2016 (cit. on p. 19).

[63] Y. Nagasaka, S. Tanaka, T. Nehira, and T. Amimoto, "Spontaneous emulsification and self-propulsion of oil droplets induced by the synthesis of amino acid-based surfactants," *Soft Matter*, vol. 13, no. 37, pp. 6450–6457, 2017 (cit. on p. 19).

[64] M. L. Morris, L. M. Baird, A. Panigrahi, M. C. Gross, R. M. Deacon, and J. J. Benkoski, "Surfactant sculpting of biologically inspired hierarchical surfaces," *Soft Matter*, vol. 9, no. 41, pp. 9857–9866, 2013 (cit. on p. 19).

[65] C. Costagliola, F. Semeraro, L. Zeppa, *et al.*, "Some physicochemical remarks on spontaneous emulsification of vitreal tamponades," *BioMed Research International*, vol. 2014, 2014 (cit. on p. 20).

[66] P. Jiang and M. J. McFarland, "Large-scale fabrication of wafer-size colloidal crystals, macroporous polymers and nanocomposites by spin-coating," *Journal of the American Chemical Society*, vol. 126, no. 42, pp. 13 778–13 786, 2004 (cit. on p. 20).

[67] C. Deleuze, B Sarrat, F. Ehrenfeld, S Perquis, C. Derail, and L. Billon, "Photonic properties of hybrid colloidal crystals fabricated by a rapid dip-coating process," *Physical Chemistry Chemical Physics*, vol. 13, no. 22, pp. 10 681–10 689, 2011 (cit. on p. 20).

[68] K.-Q. Zhang and X. Y. Liu, "Controlled formation of colloidal structures by an alternating electric field and its mechanisms," *The Journal of Chemical Physics*, vol. 130, no. 18, p. 184 901, 2009 (cit. on p. 20).

[69] Z. Li, J. Wang, and Y. Song, "Self-assembly of latex particles for colloidal crystals," *Particuology*, vol. 9, no. 6, pp. 559–565, 2011 (cit. on p. 20).

[70] V. Starov, "Nanoscience: Colloidal and Interfacial Aspects," in CRC Press, New York, 2010, ch. 15: Interactions between Particles at a Fluid Interface, pp. 397–435 (cit. on p. 20).

[71] I. B. Liu, N. Sharifi-Mood, and K. J. Stebe, "Curvature-driven assembly in soft matter," *Philosophical Transactions of the Royal Society A: Mathematical, Physical and Engineering Sciences*, vol. 374, no. 2072, p. 20 150 133, 2016 (cit. on p. 20).

[73] T. Kohyama and G. Gompper, "Defect scars on flexible surfaces with crystalline order," *Physical Review Letters*, vol. 98, no. 19, p. 198 101, 2007 (cit. on p. 20).

[74] A. Bausch, M. J. Bowick, A Cacciuto, *et al.*, "Grain boundary scars and spherical crystallography," *Science*, vol. 299, no. 5613, pp. 1716–1718, 2003 (cit. on p. 21).

[75] X. S. Ling, "Scars on a colloidal crystal ball," *Nature Materials*, vol. 4, no. 5, pp. 360–361, 2005 (cit. on p. 21).

[76] H. González-Ochoa and J. L. Arauz-Lara, "Spontaneous two-dimensional spherical colloidal structures," *Langmuir*, vol. 23, no. 10, pp. 5289–5291, 2007 (cit. on pp. 21, 31).

[77] J. Santana-Solano, C. M. Quezada, S. Ozuna-Chacón, and J. L. Arauz-Lara, "Spontaneous emulsification at the water/oil interface," *Colloids and Surfaces A: Physicochemical and Engineering Aspects*, vol. 399, pp. 78–82, 2012 (cit. on p. 21).

DIFFUSION IN NON EQUILIBRIUM SYSTEMS

As already mentioned in the previous chapter, some characteristics of the water/dodecane/span 80 system have been studied in our laboratory before starting this thesis work. In summary: the system presented spontaneous emulsification, the droplets on a curved interface self-assembled into a crystalline structure and the droplets size changes as a function of time regulated by the surfactant concentration. However, it was also interesting to know how the droplets moved along the interface on their way to their final position in the crystal structure.
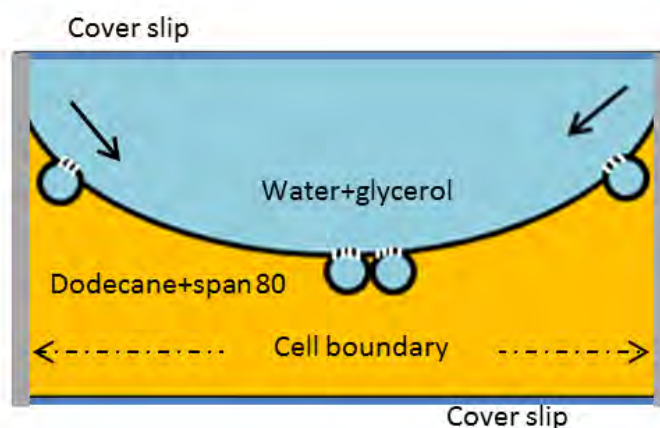
Figure 4.1: The study system is an interface between water an oil, where water droplets are generated spontaneously.

Our system is a complex system: water droplets are generated spontaneously at a spherical-like interface between water and oil. The interface appears when putting water on oil with an added non-ionic surfactant. Since the water density is greater than that of oil, the interface is produced into the oil. The spontaneously formed water droplets move attached to the interface (as is sketched in fig. 4.1 with disconti- nuous lines) while still growing from submicron sizes to a few microns. The droplets' diffusion is anisotropic due to the preferential direction of motion from the meniscus upper part to the lower meniscus part, as is sketched with the arrows in fig. 4.1. The droplets sediment at the bottom of the meniscus and forming a crystalline structure (CS), that grows as a consequence of the addition of new

droplets and also the droplets growing of the ones that form part of the structure. As a result, the CS boundary that works as a wall is not in the same position over the time. Although the process under investigation here is a complex process due to involves the movement of colloidal species through a heterogeneous dynamic medium while also changing themselves, our findings demonstrate that quantities like the mean square displacement can be accurately described by a simple model of a superposition of Brownian motion and a drift velocity. So, we do not find anomalous diffusion.

When we study diffusive behaviour in a complex environment, the objective is evaluate trajectories that usually contain more information than just the mean square displacement [78]. In various complex systems anomalous diffusion has been observed. One of the great challenges in the field of anomalous diffusion is to understand the mechanism that causes the anomalies. These devations from the expected behaviour are explained as consequences of various factors, such as the internal composition of the fluid in which the particles are suspended, the presence of some type of confinement or limitation [29], [30], [79], the medium's viscoelastic properties [80]–[82], turbulence [83], [84], inhomogeneities in the medium [85], [86], etc.

The biology field is particularly intrigued by the investigation of the movement of colloidal probes in complex environments. For example, anomalies have been observed in the lateral motion of protein intramembrane complexes, which have been attributed to their interactions with the structure of the cell cytoskeleton [27], [28], [87]. As part of these inquiries, there is growing interest in studying the diffusion process on curved surfaces, an area of significant importance on its own [88]–[90]. Additionally, the motion of colloidal species in non-equilibrium media is also a topic of interest for researchers [91]–[93].

4.1 METHODOLOGY

As we mention in chapter 3, the spontaneous emulsification process only happens in some specific liquids combination. In our case, we investigate water, dodecane and Span 80. Samples were prepared using dodecane (purity > 99%, Sigma), sorbitan mono-oleate (Span 80, purity > 99%, Sigma), pure water (resistivity 18.2 $M\Omega cm$, Mili-Q), glycerol (purity > 99%, Sigma) and a home made cell. The cell was made of stainless steel bar with dimensions $7.5cm \times 2cm \times 0.2cm$. Two concentric cylindrical chambers were drilled in the center and across the

side with the largest bar area, the top one of diameter 1.2 *mm* and height 1.85 *mm* and the bottom one with diameter 4 *mm* and height 0.15 *mm*.

The cell is reusable and the cleaning process consisted of 2 cycles of 10 minutes each in ultrasonic bath, the first with ethanol and the second one with a 2% (w/w) aqueous detergent(Micro, Cole Parmer) solution. Afterwards, 4 rinses with fresh water and finally drying with napkins (Kimwipes, Kimberly-Clark) and nitrogen, paying special attention to ensure that there is no trace of water inside the chambers. Before the cell filling process, the top surface was sealed using a circular 0.17 *mm* thick glass cover slip and epoxy resin.
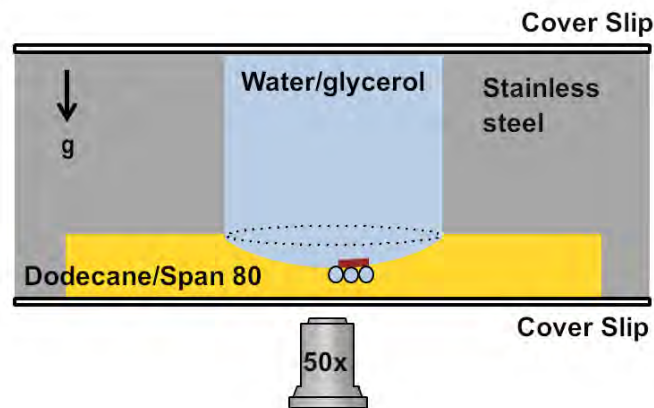
Figure 4.2: Side view of the sample cell. The interface between water/glycerol and oil/span 80 can be considered as a spherical surface cap. Adapted with permission from [94]. Copyright 2022 by the American Physical Society.

Once the epoxy resin has dried, 1.2 *μl* of water mixed with 1% (w/w) of glycerol was placed first in the upper chamber, while 2.2 *μl* of dodecane mixed with 2% (w/w) Span 80 was placed after in a gentle way. Afterwards, the second cell chamber was sealed using again epoxy resin and a circular cover slip glass with 12 *mm* of diame- ter, which was slid over the stainless steel bar avoiding disturbing the interface. Next, the cell was carefully rotated so that the aqueous phase was located at the top and oily phase at the bottom. As seen in the fig. 4.2, the final interface configuration is a convex meniscus of water into the oil with approximately $50 - 115\,\mu m$ height. Right after preparing the sample cell, we observed the meniscus using an inverted optical microscope (Olympus IX71) with a 50X objective (NA 0.5). To acquire images, we utilized a CMOS camera (Thorlabs DCC3240M) at 22.9 fps, so that $\Delta t = 0.0436\,s$, and spatial resolution of 1024×1280 pixels. To get the frames from the *avi* video obtained with the camera, we use

the software Virtual Dub.

The time analysed in each experiment sequence was $\approx 131\,s$, time in which we consider that the crystal-like structure boundary remains approximately in the same place. The image tracking was perform using the pluggin Mosaic included in Image J [95]. It is necessary to mention that glycerol is used to slightly increase the aqueous phase viscosity, so that longer trajectories are obtained in the time analysed than in the case without glycerol. Finally, we used a custom home made algorithm implemented in Fortran 90 for the analysis of the trajectories and to calculate the mean displacement (eq. 4.1), jump distribution and mean square displacement (eq. 4.2).

$$\langle [\Delta x(n\Delta t)] \rangle = \frac{1}{N-n} \sum_{i=1}^{N-n} (x_{i+n} - x_i) \tag{4.1}$$

where N is the trajectory length, n is the lag time and x_i are the droplet's positions.

$$\langle [\Delta x(n\Delta t)]^2 \rangle = \frac{1}{N-n} \sum_{i=1}^{N-n} (x_{i+n} - x_i)^2 \tag{4.2}$$

The experimental details about the meniscus shape and the analysis of the droplet's trajectories are described in appendix A.

4.2 STUDY MODEL DESCRIPTION

As soon as the liquids come into contact the emulsification process starts, due to the surfactant lipophilic nature we observe water droplets in dodecane. As it is described in subsection 4.2.1, in contrast with other similar experiments, we observe that the droplets remain attached to the interface and growth as a function of time and the surfactant concentration. Moreover, we observe that the droplets in this configuration move from the upper to the lower meniscus part and have similar size that allows the formation of a very well defined crystalline structure as showed in fig. 4.3a. The corresponding Fast Fourier transform is in fig. 4.3b, where it can be identified the typical arrangement of peaks in an hexagonal ordered configuration.

The behaviour described above, characteristic of our system, can be compared with the experiment reported by Bochner de Araujo and co-workers [96]. They investigate spontaneous emulsificaton in the
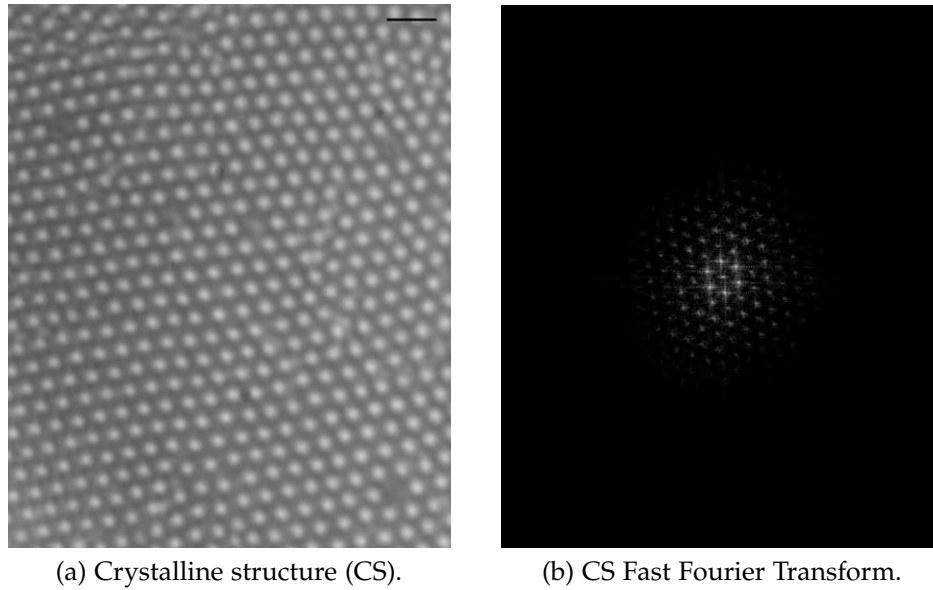
(a) Crystalline structure (CS).   (b) CS Fast Fourier Transform.

Figure 4.3: Droplets self-assemble in a crystalline structure at the meniscus bottom. The bar at the upper left corner of figure (a) is $5\,\mu m$.

system water/toluene/asphaltene and use a similar configuration cell made by glass filled in a way that water is at the bottom and oil in the upper part. The amount of liquid is greater than what we use, $100\,\mu l$ of water and $30\,\mu l$ of toluene/asphaltene solution. Although both experiments have similar shape interfaces, and we observe the droplets movement towards the center of the meniscus, there are some differences: 1)the droplets have different sizes in the case of Bochner de Araujo, so they didn't observe crystalline structure. 2)In the Bochner de Araujo work the droplets at the bottom experiment a degree of coalescence and they don't report the increasing in droplets size. We can explain this differences as follows: the capillary stainless steel walls confine the interface to a meniscus cap and the junction boundary between the liquids and the cell is a zone of emulsification (fig. 4.4a). Thus, the droplets move from the upper to the lower meniscus part. Also, in the Bochner de Araujo work the interface is almost a sphere without near walls and only attached to a capillary that supplies the water to the droplet. So, we can infer that confinement is relevant in this experiment, also the surfactant that confers stability to the droplets and prevents coalescence. We will continue to talk about the system peculiarity in the next subsection 4.2.1, where we discuss about the results when some aspects in the original experiment are changed.

On the other hand, regarding the droplets increasing size [76], a proposed mechanism is that the droplet's interface is not a surfactant monolayer [97], instead, it is conceived as a mixture of surfactant, water and oil as sketched in fig. 4.4a. As previous work in our laboratory explains [98], the droplets grow because they are still part of the interface (fig. 4.4b). The water accumulated in the surfactant layers form a kind of liquid bridges, which are supported by a balance between wetting and surface tension. The droplets are formed due instabilities in the liquid bridges driven by capillary forces.
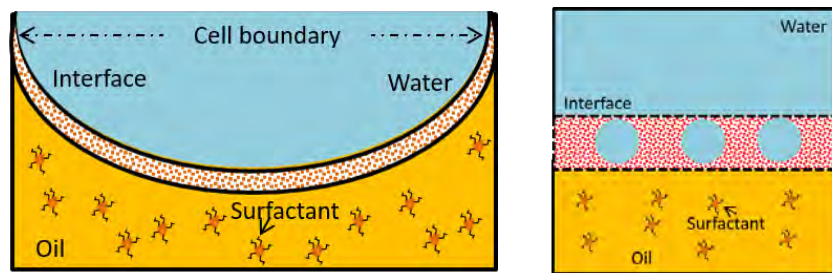
(a) A multilayer of surfactant forms at the interface between water and oil after sample preparation.

(b) Droplets are formed due to instabilities in the liquid bridge.

Figure 4.4: Proposed mechanism for emulsification and for which droplets remain attached to the interface.

4.2.1   *System peculiarity*

As we mention before, our study system is peculiar due the phenomenons that happen at the interface, not only the spontaneous emulsification but also the self-assembly structures observed. In the original experiment, the droplets self-assembled in a crystalline structure. At first sight, the principal cause is the interface shape, but if we use the same interface shape between water/dodecane, but instead of surfactant we add polystyrene particles (1.5 μm, $\phi = 0.01$), the particles are ordered at the interface in a monolayer with a kind of spread hexagonal array (fig. 4.5a), in the same way it is reported in the literature, under the name of repulsive crystals [35]. This is due to the existence of residual surface charges at the particle-oil surface, charges that do not exist in the case of emulsion droplets. So that the surfactant nature (neutral charge) and its interaction with the phases is relevant.

If the shape of the cell is changed, as it's described in subsection 5.1.2 (where the interface is not affected by gravity, fig. 4.5b) we find

different scenarios in the droplets behaviour: 1)The water droplets do not remain attached to the interface, as soon as the droplets are formed they move by diffusion away from the interface into the oily phase. 2)As it is described in section 5.4, inverse droplets are formed near the interface and sometimes they are arranged in a monolayer crystalline structure with hexagonal array parallel to the interface (fig. 4.5c). So, as we can expect, the CS depends on the shape of the interface.
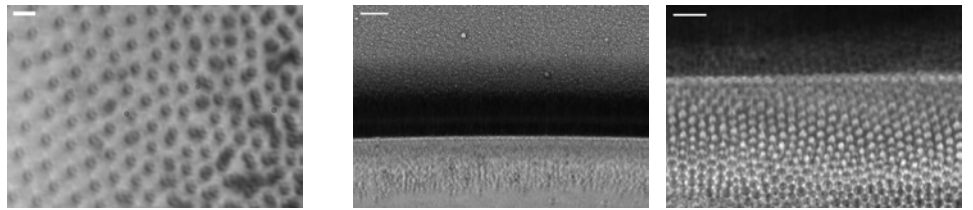
(a) Polystyrene particles at curved water/dodecane interface. Scale bar is 5 μm.

(b) Spontaneous emulsification in quasi 2D cell. Scale bar is 10 μm.

(c) Crystalline structure in quasi 2D cell. Scale bar is 10 μm.

Figure 4.5: The study system is peculiar not only for the spontaneous emulsification but also for the CS formed during the process. Particles in a similar configuration at curved interface formed a kind of repulsive crystal, while the same system but in a different configuration still formed a CS.

4.3 DROPLETS SELF-ASSEMBLY IN THE CRYSTALLINE STRUCTURE

The droplets generated by spontaneous emulsification remain attached to the interface and move along the interface from the top to the bottom of the meniscus. The droplets settle at the bottom and, since they are of similar size, form a crystalline structure (CS). The CS has an hexagonal packing and, due to confinement effects and curvature [72], presents defects sequences with coordination numbers five, seven and even eight (as is showed in appendix B.4).

A sequence of pictures of the CS growth is shown in appendix B.2. The CS has a circular geometry, the droplets self-assembled in circular layers centered within the confinement imposed by the cell. CS grows until the droplets cover the total interface. This is due to two reasons: 1)more droplets are added to the structure, 2)the droplets that are already part of the structure increase their size. It is also observed that droplets are produced faster at the beginning of the process than at the later times. Although not all experiments are exactly
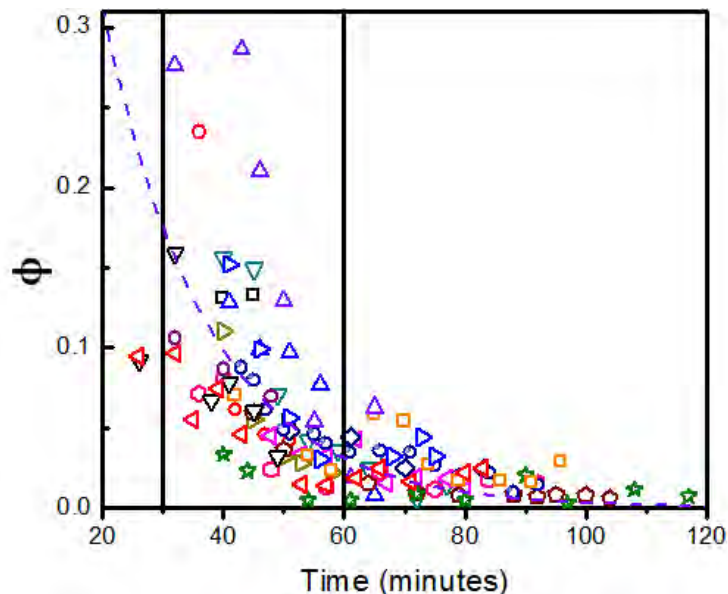
Figure 4.6: The area fraction ϕ of the droplets that approach the crystalline structure (open symbols) for different experiments (each represented by a different color) decreases as the time of the experiment progresses (dashed line). This behaviour allows to differentiate the intermediate and final stages in the CS formation.

the same quantitatively, since the experiment is an out-of-equilibrium process and it depends on the initial conditions, in general one can distinguish three CS formation stages. The nucleation stage was qualitatively determined as the one in which sedimented droplets were clearly observed forming a small CS with a defined center.

On the other hand, intermediate and final stages of CS formation were differentiated taking account the number of droplets moving to the CS in terms of their area fraction. The experimental details about this calculation are described in appendix B.3. As can be seen in fig. 4.6 the experimental data for the area fraction ϕ of the droplets moving to the CS (open symbols) of different experiments (each one of different color) decrease exponentially as a function of time, clearly described by the fit (dashed line), $\phi = exp(-0.058t)$. As described in section 4.2, we propose that the droplets remain as a part of the interface. Furthermore, once formed, they associate with all the necessary surfactant molecules which are redistributed as the droplets grow. This means that the available surfactant molecules (those that are not part of the droplets could be in the cell walls or in micelles in the solution), are being incorporated to the interface as the experiment progresses. Therefore, the number of droplets that add to the CS probably decreases because the available surfactant molecules to

form new droplets are almost finished. Each stage is briefly described below:

- **Nucleation.** It happens between 0 and 30 minutes. Several small droplets ($d < 1\,\mu m$) are observed to be organized at the interface lower part defining what will be the center of the colloidal crystal.

- **Intermediate stage.** The time period is approximately between 30 and 60 minutes. The CS growth is mainly due to the annexing of new droplets ($d \approx 1\,\mu m$), the number of droplets increases compared to the previous stage. In fraction area terms, obtained as described in appendix B, ϕ decreases from 0.3 to 0.05.

- **Final stage.** During this stage ($t > 60$ minutes) CS growth mainly by the increase in size of the droplets that are already in the structure and only few new droplets ($d \approx 1\,\mu m$) are annexed to CS, i.e. $\phi < 0.05$.

4.3.1 *Droplets adhesion force to the interface*

As we mention previously, one system's characteristic is that the droplets remain attached to the interface, as a result the droplets increasing their size as a function of time. We did the follow-up for several days of droplets growth, in most of the experiments the cell was perturbed and the CS collapsed. The observation period was between $1 - 29$ days (not the same for all experiments).
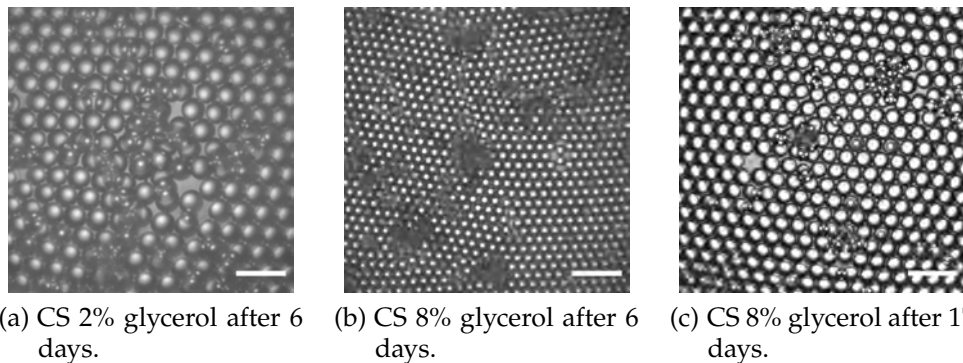

(a) CS 2% glycerol after 6 days.

(b) CS 8% glycerol after 6 days.

(c) CS 8% glycerol after 17 days.

Figure 4.7: Droplets growth is slower in the presence of glycerol in aqueous phase. Scale bar is $30\,\mu m$.

On the other hand, we observe that the droplets growth with glycerol in the aqueous phase is slower than in the case without glycerol. As an example, in figures 4.7a and 4.7b is showed the comparison

between droplets with 2% and 8% of glycerol after six days in both cases, while in figs. 4.7c is the same experiment with 8% of glycerol after 17 days. Some areas of the CS looks darker due the black layer caused by the saturation of inflated micelles [99], it means the original droplets have *daughter droplets*. The slow growth is due to the lower permeability of glycerol in membranes than in the pure water [100]. So, if we stablish that the interface in the studied system is similar to a membrane, the permeability of the mixture will be smaller than the water alone.

After 29 days, we observe the maximum droplets size: $d \approx 30 \, \mu m$, size in which droplets detach from the interface and fall to the cell bottom. Assuming that practically we have water droplets ($\rho_{water} = 997 \, kg/m^3$) in dodecane ($\rho_{dodecane} = 749.5 \, kg/m^3$), from a mechanical point of view, the forces acting on the droplets are in equilibrium, we can calculate the *adhesion force*, F_{ad}, of one droplet in the meniscus center, as follows:

$$F_{ad} = W - F_b \tag{4.3}$$

where W is the droplet weight and F_b is the bouyance force. For one droplet in the CS in intermediate stage ($d \approx 1 \, \mu m$), we have $F_{ad} \approx 0.01 \, pN$, while just before the droplet separate from the interface $F_{ad} \approx 66 \, pN$. These values are in the range, for example, of reported values of attractive radial force between uncharged colloidal particles trapped in flat water/air intefaces [101], the force between a charge colloidal particle and a wall [102], and the attractive force between magnetic micro particles [103].

4.4 DROPLET MOTION AT THE INTERFACE: SINGLE TRAJECTORY ANALYSIS

Among the most commonly used particle detection-based techniques are Single Particle Tracking (SPT) methods. They have become a very powerful tool for the study of process dynamics that span a wide range of temporal and spatial scales. Particularly, SPT methods are highly used in biology, for example, inside the cell [104]. The interior of the cell is however crowded, i.e. full of obstacles, binding sites, moving parts, active pumps and other intracellular machinery and particles can undergo different behaviours, product of their interaction with the different components of the cellular interior. As an example, in a work by Maucort et al [105], they showed the vesicles

dynamics in neuroendocrine cells oscillates between periods with different diffusivity or between diffusive periods movement and active transport. It is clear then, that an analysis that averages the information throughout the entire trajectory will lead to results that are not representative of reality. Hence the importance of single particle analysis, which has become a standard tool for probe local physical properties of complex systems. The trajectories of individual particles have encoded information both on the mechanism of movement and on the environmental conditions in which they occur.

We are interested in the droplets dynamics at the interface. To describe the droplets motion, we choose the CS final stage formation, where only few droplets are added. Therefore, the droplets motion is in a dilute environment, taking as a line of reference the CS boundary (fig. 4.8a). As was described in the previous section 4.3, the CS grows as a consequence of the increase in the droplet's size, so the CS boundary is not fix. The time intervals analysed depend on this system's characteristics. In the data reported here, the interval was 3000 frames, approximately 131 s, time in which it is assumed that the CS boundary remains about the same place. In order to obtain long trajectories in the same time, we change the viscosity of aqueous phase adding 1% w/w glycerol ($\eta_{aqueousphase} = 1.029\,cp$) [106]. In fig. 4.8b are shown examples of typical trajectories in the system, from these trajectories it's possible to extract system information: 1)the droplets motion far from the CS boundary is a combination between a drift velocity and random component, 2)each trajectory is unique due to the non-homogeneity of the interface, 3) droplets velocity decreases as they approach to CS boundary.

The depicted fig. 4.8a provides a closer look at the border of the CS, as well as a few some individual water droplets descending toward the CS. These droplets were approximately $0.80 - 1.15\mu m$ in size at the moment captured (72 minutes). Here, the x direction is set pointing along the local direction of the interface and the y direction is pointing along the corresponding meridian. On the other hand, fig. 4.8b shows representative trajectories of water droplets moving at different times in the area of fig. 4.8a. Radius of the CS is about 80 μm at the time of observation. The angle α for the meniscus height (as described in appendix A.1) is about 0.201 rad. This means that in this area the component of the gravity along the surface is quite small (appendix A.1.1).

The droplets do not just sediment directly towards the bottom of the curved interface between water and oil. As it is described in the
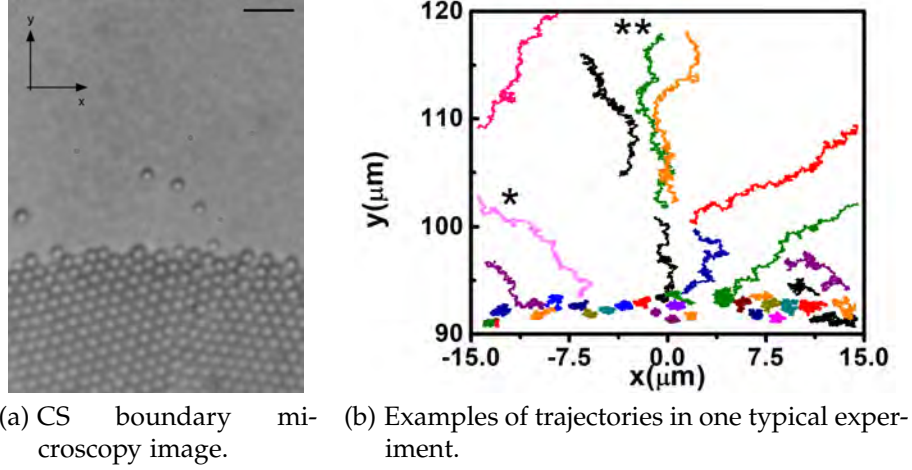
(a) CS   boundary   microscopy image.

(b) Examples of trajectories in one typical experiment.

Figure 4.8: Typical experiment (a)microscopy image, the scale bar is $5\,\mu m$. (b)same experiment trajectories. Since each trajectory is unique, single trajectory analysis is applied. Adapted with permission from [94]. Copyright 2022 by the American Physical Society.

reference [94], the trajectories show that the motion of each droplet appears to be composed of noisy straight lines of varying direction and time span (fig. 4.8). Moreover, the composition is different for different trajectories, most likely reflecting that the interface between water and oil is not homogeneous and undergoes a dynamical process.

4.4.1 *The analysis of the trajectories*

We make the assumption that the movement of the droplets obeys this simple model,

$$\Delta\vec{\mathbf{r}}(t) = \Delta\vec{\mathbf{r}}_{\mathbf{B}}(t) + \vec{\mathbf{v}}t, \tag{4.4}$$

where $\Delta\vec{\mathbf{r}}(t)$ is the particle's displacement along the interface at time t, $\Delta\vec{\mathbf{r}}_{\mathbf{B}}(t)$ represents the noise in the trajectory and $\vec{\mathbf{v}}$ is a constant representing a drift velocity. From eq. 4.4 it follows that the total mean displacement is $\langle\Delta\vec{\mathbf{r}}(t)\rangle = \langle\Delta\vec{\mathbf{r}}_{\mathbf{B}}(t)\rangle + \vec{\mathbf{v}}t$. For the moment, we are procee- ding under the assumption that the fluctuations in the particles' movement is indeed a Brownian displacement resulting from the thermal fluctuations in the surrounding environment. As a result, when considering individual droplets that are distant from the crystalline structure's border, the first moment of the Brownian displacement should be $\langle\Delta\vec{\mathbf{r}}_{\mathbf{B}}(t)\rangle$ vanishing small compared to $\vec{\mathbf{v}}t$. Therefore, $\langle\Delta\vec{\mathbf{r}}(t)\rangle = \vec{\mathbf{v}}t$. The second moment is expected to be determined by

$\langle[\Delta\vec{\mathbf{r}}_{\mathbf{B}}(t)]^2\rangle = 4D_{\parallel}t$. In this complex environment $D_{\parallel}$ represents the diffusion constant of the water droplet, named for simplicity as D. Assuming also that the Brownian and the systematic displacements are uncorrelated, the mean square displacement of single droplets should be,

$$\langle[\Delta\vec{\mathbf{r}}(t)]^2\rangle = 4Dt + (vt)^2, \tag{4.5}$$

with $v = |\vec{\mathbf{v}}|$. Since the drift velocity may change, both in direction and magnitude, in order to apply eq. 4.4 the trajectories are sectioned accordingly as we described in appendix A.3. This method was applied to analyse the movements of numerous droplets within the same system, as well as in different realizations of it. It is found that the motion of the droplets was consistently comparable in all cases, though there was some dispersion in the quantitative results, likely due to the process taking place under non-thermal equilibrium conditions. To avoid confusion, we have chosen to present and examine the results for only one single droplet. However, it is important to note that the findings for the other droplets are qualitatively identical. In appendix B.1 is shown another example of trajectory analysis, the droplet with double asterisk in fig. 4.8b.
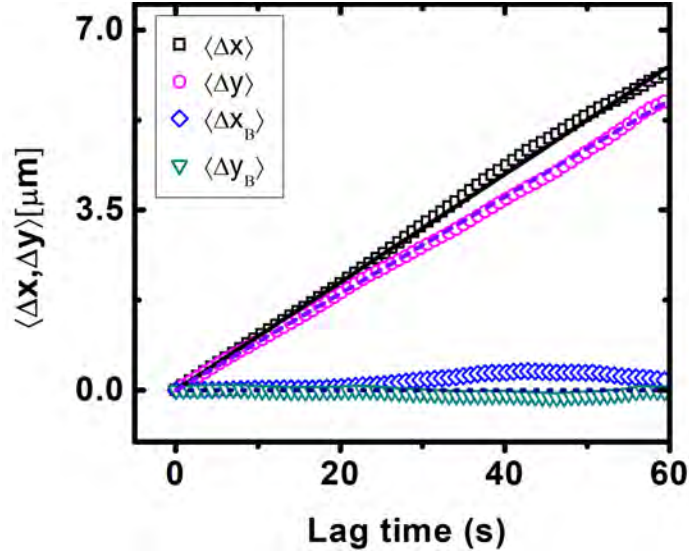
Figure 4.9: Droplet's mean displacement total (squares and circles) and Brownian (diamonds and triangles) along directions x and y, respectively. Adapted with permission from [94]. Copyright 2022 by the American Physical Society.

Fig. 4.9 illustrates the time-dependent mean displacement values of the displacement components $\Delta y(t)$ and $\Delta x(t)$, derived from the tra-

jectory marked with an asterisk in the previous fig. 4.8b. These average is computed solely based on the data from this single trajectory. Both components (square and circle symbols) are well-suited to linear fits, as shown by the solid and dashed lines, which supports the assumption that $\langle \Delta \vec{r}_B(t) \rangle$ is vanishing small. Consequently, we can derive the components of the drift velocity, v_x and v_y, from the linear fits. As the trajectory in this case is at an angle of roughly $45°$ with respect to the vertical, both components are nearly identical. Building on the analysis of the trajectory, we can use eq. 4.4 to determine the noisy component of the displacement as $\Delta \vec{r}_B(t) = \Delta \vec{r}(t) - \vec{v}t$. The mean values of this noisy component are presented in fig. 4.9 (diamonds and triangles), exhibiting that indeed these quantities are vanishing small along both directions.
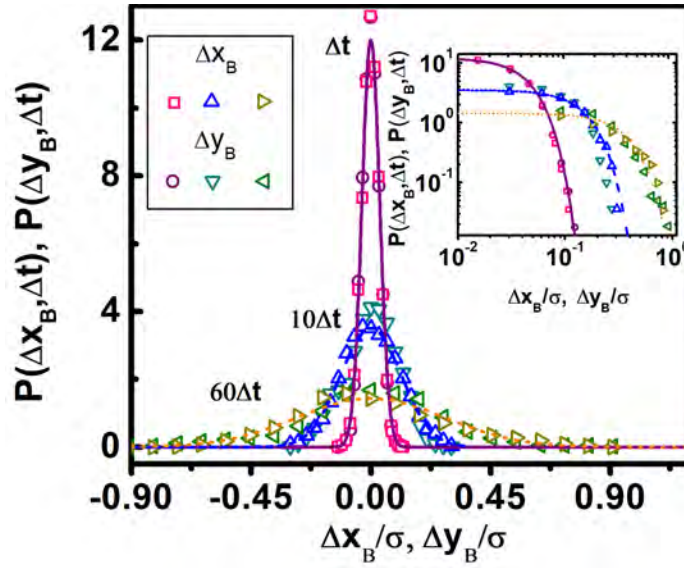
Figure 4.10: Step distribution functions of the Brownian displacements at three times. The data is represented by symbols and is compared to the theoretical predictions given by eq. 4.6 (lines). The inset of the plot displays the distribution function for only positive displacements on a logarithmic scale. Adapted with permission from [94]. Copyright 2022 by the American Physical Society.

In fig. 4.10 the experimental distribution functions of steps at three different times ($\Delta t = 0.0436\,s$ as is mentioned in section 4.1) $t = \Delta t$, $t = 10\Delta t$ and $t = 60\Delta t$ (symbols) are presented. The shape and symmetry of these functions are similar to the way a single particle diffuses with a diffusion constant D in a fluid that is in thermal equilibrium, which represents the distribution of steps x, characterized by the Gaussian function,

$$P_G(x, t) = \frac{1}{\sqrt{4\pi Dt}} exp\left[-\frac{x^2}{4Dt}\right] \qquad (4.6)$$

In fig. 4.10, the solid and dashed lines represent plots of the Gaussian function given by eq. 4.6. These lines correspond to the experimental times, and the value of the constant D has been adjusted to fit the experimental data at $t = \Delta t$. The experimental distribution functions are described quite precisely, quantitatively and qualitatively, in time and space, by the same Gaussian function with zero mean value and variance $\sigma^2 = 2Dt$. The step distribution functions along both the independent x and y directions are identical, and they expand in time with the same diffusion coefficient. For the trajectory analysed in this part, it is found from the fits that $v_x = 0.105 \mu m/s$, $v_y = 0.093 \mu m/s$, $D_x = 1.5 \times 10^{-2} \mu m^2/s$ and $D_y = 1.4 \times 10^{-2} \mu m^2/s$. The value of D used here is the average of D_x and D_y.
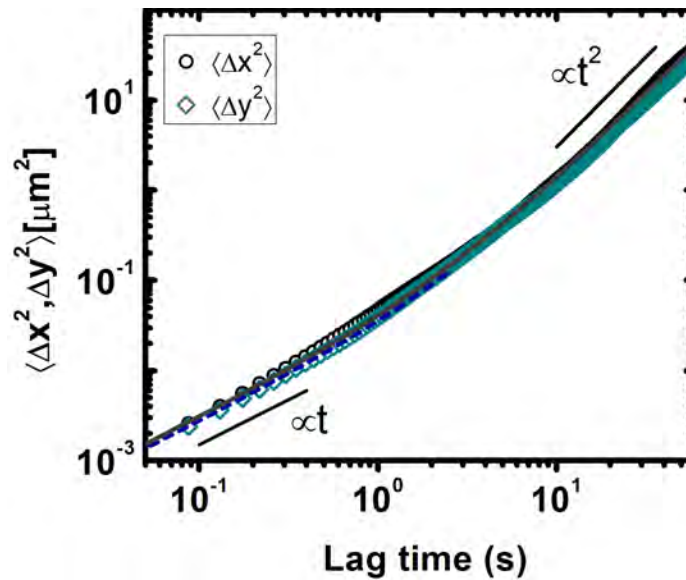
Figure 4.11: Mean squared displacement along x and y directions (symbols) correspond to the experimental results and lines are eq. 4.5 using the fitting values for velocity components and diffusion constant obtained from the data in fig. 4.9 and 4.10, respectively. Adapted with permission from [94]. Copyright 2022 by the American Physical Society.

The velocity and diffusion constant obtained from the fitting process can be used as inputs for eq. 4.5. This allows the calculation of the mean square displacement, which can then be compared to the experimental data. Fig. 4.11 displays the components of the mean square

displacement, for both the x and y directions. The lines have been obtained from eq. 4.5. The experimental data is also represented on the plot by open symbols. The level of agreement between the experimental data and eq. 4.5 is quite remarkable, spanning a broad range of time that covers three decades. Initially, mean square displacement have a linear regime, followed by regime where the quadratic term becomes more significant and starts to dominate. At short times, the experimental data for both components of the mean square displacement are the same. However, at longer times, the values differ slightly due to differences in the velocity components.

It is possible to input the values obtained for the velocity and diffusion constant into eq. 4.6 and calculate the distribution function of the variable $x + vt$, which is represented as $P_G(x + vt, t)$. Plots of this function at three times, using v_y and D_y, are shown in fig. 4.12a (lines). The distribution of the experimental displacements $\Delta y(t)$ is also shown for comparison (symbols). The comparison between the experimental results and the predictions made by equation eq. 4.6 is highly consistent and accurate. The data presented in the fig. 4.12b indicates that the experimental distribution of displacements in the x direction is in good agreement with equation 4.6.

The study of the movement of individual particles within systems that are undergoing processes out of thermal equilibrium is an area of significant current interest because it could be used to probe properties of such systems, whether they are naturally occurring or artificially created, in the same manner as it is being used in condition of thermal equilibrium. When analysing systems that are in thermal equilibrium, deviations from normal diffusion are typically attributed to the properties of the system, such as its structure. To conduct a similar analysis on systems that are out of thermal equilibrium, it is necessary to be clear first whether deviations should be expected just by the non-equilibrium conditions or those can be attributed only to other properties of the system.
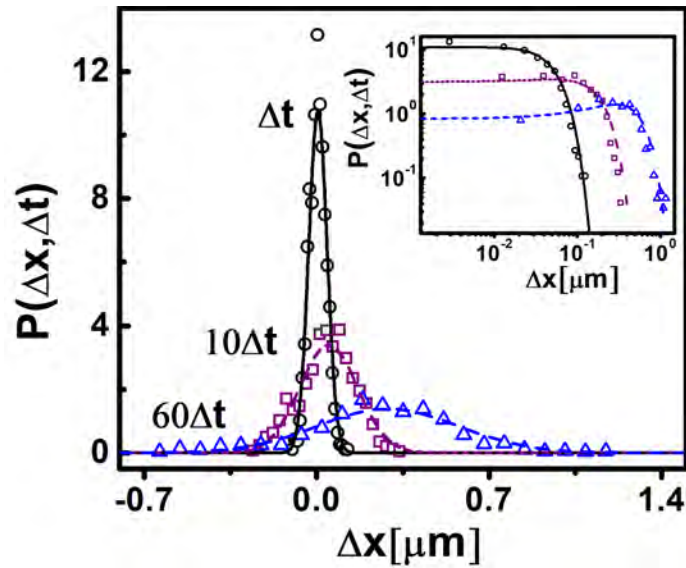
Another approach to the single trajectory analysis

As we discuss in the previous section 4.4.1, from eq. 4.4, we can find the noise in the trajectory,

$$\Delta \vec{\mathbf{r}}_{\mathbf{B}}(t) = \Delta \vec{\mathbf{r}}(t) - \vec{\mathbf{v}}t, \tag{4.7}$$
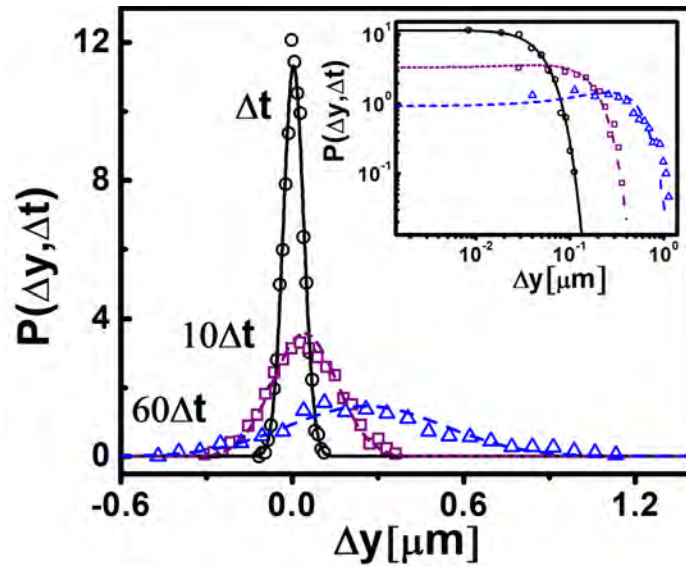
(a) Step distribution function along y direction. Adapted with permission from [94]. Copyright 2022 by the American Physical Society.

(b) Step distribution function along x direction.

Figure 4.12: The step distribution function along y and x direction at three different times, obtained experimentally (symbols) and from eq. 4.6 (lines). The inset shows the data of the distribution function only for the positive displacements in the log-log scale.

So, if we work with this *trajectory* (inset in fig. 4.13), it follows the mean square displacement is,

$$\langle [\Delta \vec{r}_\mathbf{B}(t)]^2 \rangle = 4Dt \tag{4.8}$$

where again, D is the diffusion constant of the water droplet in this complex environment. So that the constant D calculated through the fitting to the Gaussian function, eq. 4.6, must be the same as the D obtained with the linear fitting to mean square displacement (eq. 4.8) for short times. As shown in fig. 4.13 there are a good agreement with the previous values $D_x = 1.5 \times 10^{-2} \mu m^2/s$ and $D_y = 1.4 \times 10^{-2} \mu m^2/s$. The lines reproducing the behaviour of the time interval studied and the small differences are due to the fact that the average is over a finite time. In appendix B.1 the graph corresponding to the other example presented is shown, i.e., the trajectory marked with a double asterisk.
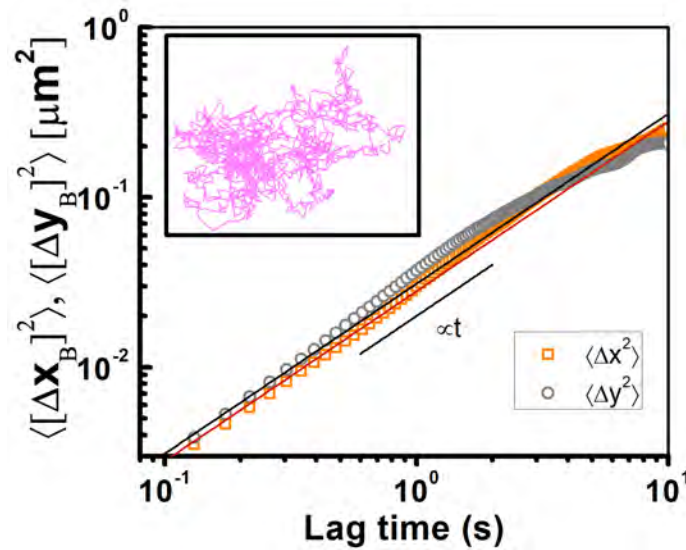
Figure 4.13: Mean squared displacement along x and y directions (symbols) correspond to the experimental results and lines are fits to eq. 4.8 where the diffusion constant is obtained. We observe a good agreement with the previous calculated values. The inset is the experimental trajectory obtained after eq. 4.7.

As shown here, the way to analyse the individual trajectories is robust and it is confirmed that the droplets exhibit a well-identified Brownian component and a drift velocity. The Brownian component with a Gaussian distribution of steps due to the thermal agitation of the media surrounding the droplets and the drift velocity due to the effect of gravity.
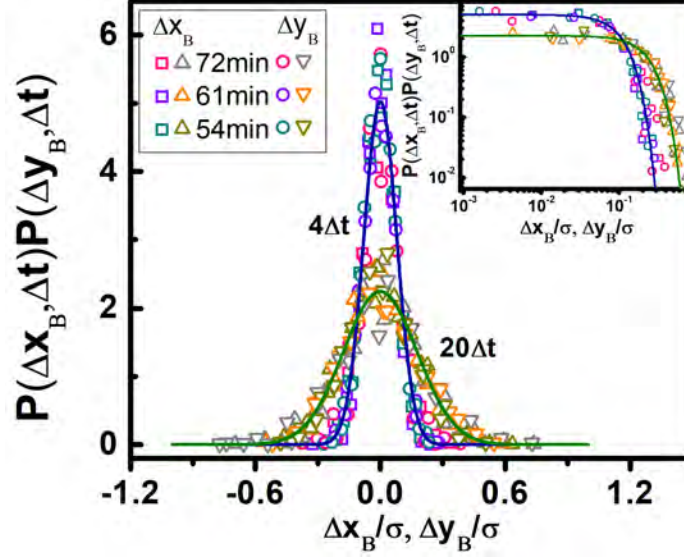
Figure 4.14: The step distribution function for Brownian displacements at $4\Delta t$ and $20\Delta t$ obtained experimentally (symbols) for three different times from the beginning of the experiment and from eq. 4.6 (lines). The inset shows the data of the distribution function only for the positive displacements in the log-log scale.

4.4.2 Diffusion coefficients

As we described in section 2.5, $2D$ diffusion of colloidal particles absorbed to an interface is a topic that has been extensively studied. By way of comparison, using typical values found in the experiments, for a free particle, radius $0.5\,\mu m$, moving in water, the diffusion coefficient is $D_{water} = 43.2 \times 10^{-2}\,\mu m^2/s$, while if the same particle were moving in dodecane the diffusion coefficient is $D_{oil} = 32.3 \times 10^{-2}\,\mu m^2/s$. For water droplets moving at an interface, the diffusion coefficients found are an order of magnitude smaller, which qualitatively agrees with the ultra-slow diffusion observed in other interfacial systems, such as proteins on cell membrane, bacteria biofilms and particles in emulsions [39]. This is, $\langle[\Delta r(t)]^2\rangle$ increases linearly with time but with a smaller slope than D_{water} and D_{oil}. Here, we will not go into the subject in depth in order to explain the origin of the extra drag force at the interface that reduces the droplet motion, which is an interesting topic in its own right. There are numerous studies in the literature, both *in situ* and *in silico*, that associated the extra drag force on the interface with the three phase contact angle, the viscosity ratio of the two fluids, the deformation of the interface, surface tension, size and density of adsorbed particles at the interface and also the presence of adsorbed surfactant at interface [107].

On the other hand, fig. 4.14 shows data on the dynamics of the droplets in one experiment at different times from its preparation $\tau = 54$, 61 and 72 minutes, in one histogram for two different times $4\Delta t$ and $20\Delta t$. The open symbols in fig 4.14 are experimental data and the lines are the representation of eq. 4.6 using the average value of diffusion coefficient, D_x and D_y of all droplets analysed. We observe a good agreement between the experimental data and eq. 4.6, which means that the droplets move over an approximately similar interface during the evolution of the last stage of the experiment.

4.5 TEMPORAL EVOLUTION OF THE DROPLET MOTION

During the experiments realizations, we identify that the velocities are slightly different during the temporal evolution of the experiments. Even when the velocities have different directions, we analyse the average behaviour of all the droplets present at different times of the same experiment $t = 57.0$, 59.3, 61.6, 72.0 and 74 minutes, in the vertical direction y. We calculate the mean square displacement of all the droplets present in the observation area far from the CS boundary, and then fitting the data to eq. 4.5. The difference is clear in some experiments, like the one shown in fig. 4.15. The values of v_y calculated are 0.29, 0.23, 0.19, 0.14 and 0.12 $\mu m/s$, respectively for the times mention before.
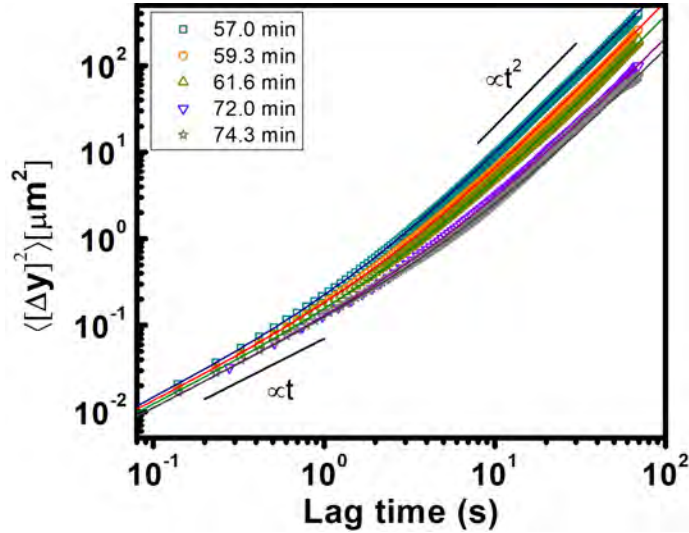

Figure 4.15: Mean squared displacement along the y direction (symbols) corresponding to the experimental results at different times from the beginning of the experiment, lines are eq. 4.5.

Even if the curvature radius of the interface increases slightly, becoming *less* flatter, perhaps due to the weight of the attached droplets,

it was observed that the droplets at short times from the beginning of the experiment move faster than the droplets present at later times. That is, the droplets velocity toward the CS is inversely related to the time since the beginning of the experiment, i.e. $v_y \propto t^{-1}$. In addition, we observe that the droplets of later times move over less free area (area without sedimented droplets, approximately half of the radius of the cell, r_{cell}) of the interface, due to the growth of the CS. Perhaps the lower velocity of the droplets gives them more time before reaching the CS boundary to reach roughly the same size as the droplets already in the structure.
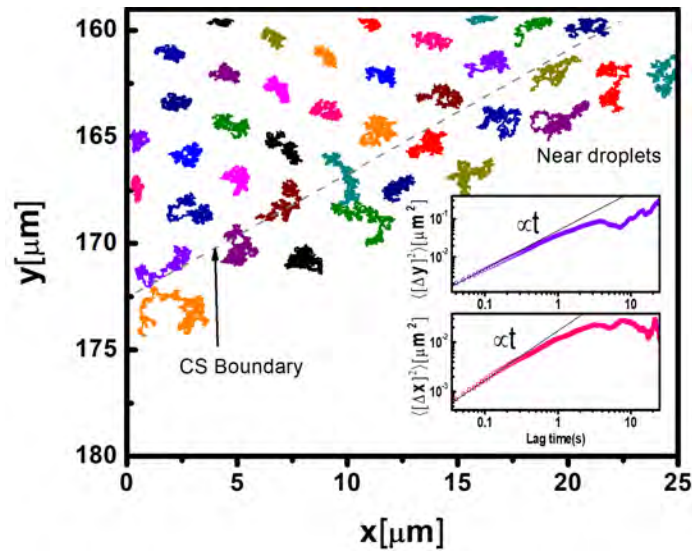
Figure 4.16: Trajectories of droplets near and in the CS structure. There are identified confined droplets in the CS and near droplets into a kind of restricted areas that escapes from the region, ending up in another. Examples of typical mean square displacement graphs are shown in the inset.

4.6 DROPLETS NEAR THE CS BOUNDARY

Regarding the droplets in the region that is close to the CS boundary, we use the single trajectory analysis again. There are interface regions where the droplets are surrounded by other droplets, the droplets in the CS structure, confining their motion to a limited part. This is illustrated in fig. 4.16, which shows examples of trajectories of droplets near and in the CS structure.

In both cases short time scales diffusion is characterized by an exponent $\alpha = 1$, i.e. normal diffusion, the difference is in longer times. The motion of droplets in CS structure is clearly restricted, allowing it

to access only part of the interface surface. The confinement continue over a long period, so the mean square displacement converge to a constant value ($MSD(t) \propto t^0$) as is shown in pink inset graph of fig. 4.16.

In the case of droplets near the CS boundary we observe two cases: 1)droplets that moving around their final position in the CS, but there aren't totally confined and 2) droplets confined between different regions, so that droplets *jump* between different accessible sites in the CS structure. Unlike droplets in the CS, droplets near CS, after the constant value in the MSD presents a period of diffusion again, i.e. the droplets *jump* to other region as is shown in purple inset graph of fig. 4.16.

REFERENCES

[27] K. Ritchie, X.-Y. Shan, J. Kondo, K. Iwasawa, T. Fujiwara, and A. Kusumi, "Detection of non-Brownian diffusion in the cell membrane in Single Molecule Tracking," *Biophysical Journal*, vol. 88, no. 3, pp. 2266–2277, 2005 (cit. on pp. 8, 27).

[28] J.-H. Jeon, H. M.-S. Monne, M. Javanainen, and R. Metzler, "Anomalous diffusion of phospholipids and cholesterols in a lipid bilayer and its origins," *Physical Review Letters*, vol. 109, no. 18, p. 188 103, 2012 (cit. on pp. 8, 27).

[29] D Winter, J Horbach, P Virnau, and K Binder, "Active nonlinear microrheology in a glass-forming Yukawa fluid," *Physical Review Letters*, vol. 108, no. 2, p. 028 303, 2012 (cit. on pp. 8, 27).

[30] I. Wong, M. Gardel, D. Reichman, *et al.*, "Anomalous diffusion probes microstructure dynamics of entangled F-actin networks," *Physical Review Letters*, vol. 92, no. 17, p. 178 101, 2004 (cit. on pp. 8, 27).

[72] V. Vitelli, J. B. Lucks, and D. R. Nelson, "Crystallography on curved surfaces," *Proceedings of the National Academy of Sciences*, vol. 103, no. 33, pp. 12 323–12 328, 2006 (cit. on pp. 20, 32).

[76] H. González-Ochoa and J. L. Arauz-Lara, "Spontaneous two-dimensional spherical colloidal structures," *Langmuir*, vol. 23, no. 10, pp. 5289–5291, 2007 (cit. on pp. 21, 31).

[78] R. Metzler, V. Tejedor, J.-H. Jeon, *et al.*, "Analysis of single particle trajectories: From normal to anomalous diffusion.," *Acta Physica Polonica B*, vol. 40, no. 5, 2009 (cit. on p. 27).

[79] D. M. Tartakovsky and M. Dentz, "Diffusion in porous media: Phenomena and mechanisms," *Transport in Porous Media*, vol. 130, no. 1, pp. 105–127, 2019 (cit. on p. 27).

[80] C. Lozano, J. R. Gomez-Solano, and C. Bechinger, "Run-and-tumble-like motion of active colloids in viscoelastic media," *New Journal of Physics*, vol. 20, no. 1, p. 015 008, 2018 (cit. on p. 27).

[81] J. H. van Zanten and K. P. Rufener, "Brownian motion in a single relaxation time Maxwell fluid," *Physical Review E*, vol. 62, no. 4, p. 5389, 2000 (cit. on p. 27).

[82] M. Khan and T. Mason, "Random walks of colloidal probes in viscoelastic materials," *Physical Review E*, vol. 89, no. 4, pp. 042309 1–6, 2014 (cit. on p. 27).

[83] G. P. Bewley, K. Sreenivasan, and D. P. Lathrop, "Particles for tracing turbulent liquid helium," *Experiments in Fluids*, vol. 44, no. 6, pp. 887–896, 2008 (cit. on p. 27).

[84] C. Scholz, F. Wirner, J. R. Gomez-Solano, and C. Bechinger, "Enhanced dispersion by elastic turbulence in porous media," *Europhysics Letters*, vol. 107, no. 5, p. 54 003, 2014 (cit. on p. 27).

[85] S. Amitai and R. Blumenfeld, "Modifying continuous-time random walks to model finite-size particle diffusion in granular porous media," *Granular Matter*, vol. 19, no. 1, pp. 1–9, 2017 (cit. on p. 27).

[86] J. R. Howse, R. A. Jones, A. J. Ryan, T. Gough, and R. Golestanian, "Self-motile colloidal particles: From directed propulsion to random walk," *Physical Review Letters*, vol. 99, no. 4, p. 048 102, 2007 (cit. on p. 27).

[87] W. N. Everett, H.-J. Wu, S. G. Anekal, H.-J. Sue, and M. A. Bevan, "Diffusing colloidal probes of protein and synthetic macromolecule interactions," *Biophysical Journal*, vol. 92, no. 3, pp. 1005–1013, 2007 (cit. on p. 27).

[88] R. Sknepnek and S. Henkes, "Active swarms on a sphere," *Physical Review E*, vol. 91, no. 2, p. 022 306, 2015 (cit. on p. 27).

[89] I. Vladescu, E. Marsden, J Schwarz-Linek, *et al.*, "Filling an emulsion drop with motile bacteria," *Physical Review Letters*, vol. 113, no. 26, p. 268 101, 2014 (cit. on p. 27).

[90] T. Sanchez, D. T. Chen, S. J. DeCamp, M. Heymann, and Z. Dogic, "Spontaneous motion in hierarchically assembled active matter," *Nature*, vol. 491, no. 7424, pp. 431–434, 2012 (cit. on p. 27).

[91] R. N. Zia and J. F. Brady, "Single-particle motion in colloids: Force-induced diffusion," *Journal of Fluid Mechanics*, vol. 658, pp. 188–210, 2010 (cit. on p. 27).

[92] C. C. Maass, C. Krüger, S. Herminghaus, and C. Bahr, "Swimming droplets," *Annual Review of Condensed Matter Physics*, vol. 7, pp. 171–193, 2016 (cit. on p. 27).

[93] F Donado, R. Moctezuma, L López-Flores, M Medina-Noyola, and J. Arauz-Lara, "Brownian motion in non-equilibrium systems and the Ornstein-Uhlenbeck stochastic process," *Scientific Reports*, vol. 7, no. 1, pp. 1–7, 2017 (cit. on p. 27).

[94] M. d. J. Martínez-López and J. L. Arauz-Lara, "Brownian motion on an out-of-thermal-equilibrium surface," *Physical Review E*, vol. 106, no. 3, p. 034615, 2022 (cit. on pp. 28, 37–40, 42).

[95] I. F. Sbalzarini and P. Koumoutsakos, "Feature point tracking and trajectory analysis for video imaging in cell biology," *Journal of Structural Biology*, vol. 151, no. 2, pp. 182–195, 2005 (cit. on p. 29).

[96] S. Bochner de Araujo, M. Merola, D. Vlassopoulos, and G. G. Fuller, "Droplet coalescence and spontaneous emulsification in the presence of asphaltene adsorption," *Langmuir*, vol. 33, no. 40, pp. 10501–10510, 2017 (cit. on p. 29).

[97] S. Pautot, B. J. Frisken, J.-X. Cheng, X. S. Xie, and D. Weitz, "Spontaneous formation of lipid structures at oil/water/lipid interfaces," *Langmuir*, vol. 19, no. 24, pp. 10281–10287, 2003 (cit. on p. 31).

[98] H. González-Ochoa, L. Ibarra-Bracamontes, and J. L. Arauz-Lara, "Two-stage coalescence in double emulsions," *Langmuir*, vol. 19, no. 19, pp. 7837–7840, 2003 (cit. on p. 31).

[99] A. Kabalnov, "Ostwald ripening and related phenomena," *Journal of Dispersion Science and Technology*, vol. 22, no. 1, pp. 1–12, 2001 (cit. on p. 35).

[100] E. Orbach and A. Finkelstein, "The nonelectrolyte permeability of planar lipid bilayer membranes.," *The Journal of General Physiology*, vol. 75, no. 4, pp. 427–436, 1980 (cit. on p. 35).

[101] V. Carrasco-Fadanelli and R. Castillo, "Measurement of the force between uncharged colloidal particles trapped at a flat air/water interface," *Soft Matter*, vol. 15, no. 29, pp. 5815–5818, 2019 (cit. on p. 35).

[102] G. Volpe, L. Helden, T. Brettschneider, J. Wehr, and C. Bechinger, "Influence of noise on force measurements," *Physical Review Letters*, vol. 104, no. 17, p. 170 602, 2010 (cit. on p. 35).

[103] M. N. Romodina, M. D. Khokhlova, E. V. Lyubin, and A. A. Fedyanin, "Direct measurements of magnetic interaction-induced cross-correlations of two microparticles in Brownian motion," *Scientific Reports*, vol. 5, no. 1, pp. 1–7, 2015 (cit. on p. 35).

[104] C. Manzo and M. F. Garcia-Parajo, "A review of progress in Single Particle Tracking: From methods to biophysical insights," *Reports on Progress in Physics*, vol. 78, no. 12, p. 124 601, 2015 (cit. on p. 35).

[105] G. Maucort, R. Kasula, A. Papadopulos, T. A. Nieminen, H. Rubinsztein-Dunlop, and F. A. Meunier, "Mapping organelle motion reveals a vesicular conveyor belt spatially replenishing secretory vesicles in stimulated chromaffin cells," *Plos one*, vol. 9, no. 1, e87242, 2014 (cit. on p. 35).

[106] M. L. Sheely, "Glycerol viscosity tables," *Industrial & Engineering Chemistry*, vol. 24, no. 9, pp. 1060–1064, 1932 (cit. on p. 36).

[107] J. C. Loudet, M Qiu, J Hemauer, and J. Feng, "Drag force on a particle straddling a fluid interface: Influence of interfacial deformations," *The European Physical Journal E*, vol. 43, pp. 1–13, 2020 (cit. on p. 44).

ENCAPSULATION CAPACITY AND SELF-ASSEMBLY IN SPONTANEOUS EMULSIFICATION

Encapsulation strategies of species, such as colloidal particles or drugs, are made to protect the active ingredients against chemical and enzymatic degradation, aggregation, premature release in storage or processing [108]. In recent years, directed delivery and release controlled transfer of hydrophobic and hydrophilic drugs via nanocarriers is among the most widely researched topics. In particular, spontaneous emulsification has been used as a low-energy method for the synthesis of nanoparticles and as a medium to make nanoemulsions for the study of controlled release of drugs. Using SE has achieved, for example:

- Encapsulate vitamin D in nanoemulsions in which factors such as the type of surfactant [109] or the oil composition [110] influence droplet size.

- Encapsulate flurbiprofen, an anti-inflammatory drug that is poorly soluble in water, in a nanoemulsion in order to study its parenteral administration [111] unchanged chemical compositions.

In this sense, we review the encapsulation capacity of the spontaneous emulsification. Our hypothesis is that whatever the mechanism that causes spontaneous emulsification, the interface is a semipermeable membrane, it is not a single layer of surfactant but a film made up of surfactant, water and oil. The interface allows the passage of the aqueous phase to the oil phase. To find out what sizes of probe species could pass through the interface and be encapsulated in water droplets, experiments were performed in a so-called horizontal glass cell to get rid of gravity effects.

5.1 METHODOLOGY

5.1.1 *Different cell configuration in the same system*

As we described in section 3.1, spontaneous emulsification occurs in specific systems as soon as the liquids are put in contact. Figure 5.1 shows the liquids used in this study: dodecane and water $(1 : 5\ v/v)$,

in the left vial with 2% w/w span 80 and in the right one without surfactant. After 24 hours, we observe the characteristic white color of an emulsion in left vial, due to the water emulsified in dodecane while in the right one we don't observe any change. Thus, the spontaneous emulsification process is independent of the container, or the volume, but the specific droplets behaviour depends on the confinement, as it is described in section 4.2.

As proposed in the previous works in our laboratory, we worked on a curved interface under the influence of gravity and additional question arose: we think that spontaneous emulsification is a process where droplets form and swell by their communication to the aqueous phase through a kind of bridges at the interface (as we described in section 4.2), but *what would be the molecule or particle probe maximum size that could pass through the aforementioned bridges?* To try to answer this question, in addition of the stainless steel cell we use an *horizontal cell* as described below.
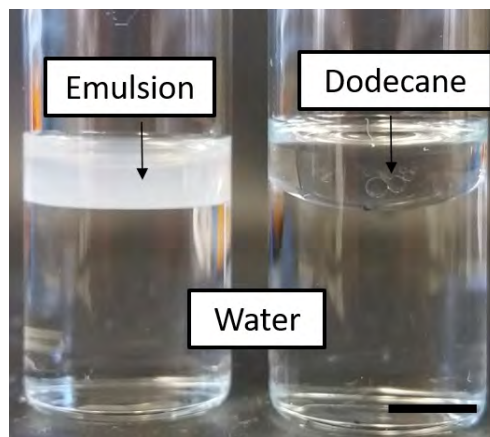
Figure 5.1: Spontaneous emulsification in bulk. Bar scale 1 *cm*.

5.1.2 *Horizontal cell*

Due to the surfactant nature, water droplets are emulsified in dodecane. In order to determine the maximum size probe that can be encapsulated by SE, we used different fluorescent species suspended in the aqueous phase. In this case, it was better to use an upright microscope, the Olympus *BX*51 where the illumination comes from the upper part and we used a CCD camera *Watec* brand (30 *fps*) adapted to take pictures of size 640×480 pixels. In contrast with the spherical-like interface experiments, the interface in these experiments is approximately flat and it is not affected directly by the gravity since the

liquids are in the same plane, as it is shown in fig. 5.2.
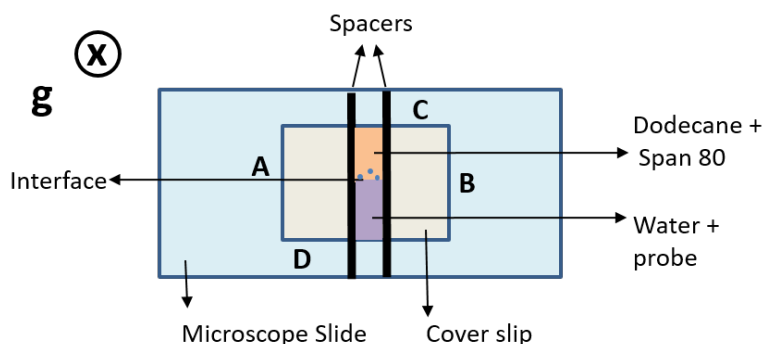
(a) Schematic top view of a quasi 2D horizontal glass cell.
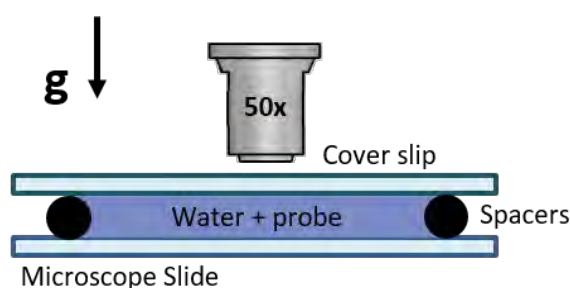
(b) Side view of the horizontal cell set up.

Figure 5.2: We explored other configuration of the same system, where the liquids are in the same plane.

The cell is usable only one time and the cleaning process consisted of 6 cycles of one hour in magnetic stirrer plate, the first with methanol and the second with a heated 2% (w/w) aqueous detergent (Micro, Cole Parmer) solution. Afterwards, 4 rinses with fresh water and finally drying with heat. The next step is the glasses silanization process using a Octadecyltrichlorosilane (OTS) solution 0.2% v/v in toluene. After 20 minutes in the aforementioned solution, the glasses are dried with nitrogen and rinsed with chloroform shaking them in ultrasonic bath during 20 minutes. Finally, the glasses are dried again with nitrogen.

Prior to filling the cell, it is necessary to assemble it (the final sample cell configuration is shown in figure 5.2a). To do this, we used cylindrical spacers of 0.2 mm in diameter and 2.5 cm of length. The spacers are first glued on the microscope slide glass. The lateral distance between spacers is 0.6 mm. The cover slip is put on the spacers and it is glued on sides A, B and half part of C and D with epoxy resin. When the epoxy resin is dried, the cell is loaded with a glass

Fluorescent species	μw/Size	Concentration
Dextran Rodhamine B	$10\,kDa$	$0.266\,mM$
Dextran fluorescein	$40\,kDa$	$0.607\,mM$
Dextran Rodhamine B	$70\,kDa$	$2.678\,mM$
$CdSe/ZnS$ nanocrystals	$6.1\,nm$	$0.036\,mM$
Polymer microspheres	$26\,nm$	$0.02\,\%\,(v/v)$

Table 5.1: Fluorescent species used in the horizontal cell set-up.

syringe (Hamilton brand). In side C it is injected the aqueous phase while in side D the oil phase. After that, sides C and D are gently and completely sealed with epoxy resin taking care not to disturb the interface. As soon as the sample cell is sealed, it is observed with the upright microscope as is shown in fig. 5.2b. The observation areas are the interface, between the dodecane+span 80 and the water+probe, and the near area to the interface both in the water and in the oil side.

5.1.3 *Probe species for study encapsulation capacity*

As it was mentioned in previous subsection, different fluorescent species are put in aqueous phase to observe the encapsulation capacity of spontaneous emulsification phenomenon. The species used as well as their concentration are listed in table 5.1.

5.2 STUDY MODEL DESCRIPTION

The main difference between the results obtained in the vertical cell (section 4.1) and the horizontal cell (subsection 5.1.2) is that the droplets in this second type of experiments do not remain attached to the interface. Once formed they are separated from it by diffusion. Also, the interface did not remain static: it changed its initial configuration by moving to the spacers. This flow, and other non-equilibrium system conditions, led to several different scenarios of droplet self-assembly (as shown in the section 5.4).

In the experiments carried out in the horizontal cell, fluorescent probe species were used to observe through fluorescence microscopy that these species crossed the interface. As described in the subsection 5.1.3 different probe species, in the range of molecules to nano-colloids, were used: dextran rhodamine B, dextran fluorescein, $CdSe/ZnS$ nanocrystals and colloidal particles. For the fluorescent dyes, different concentrations of surfactant were explored (0.25%, 1%, and 2%)

and in all cases bright droplets were observed in the oily phase. For the *CdSe/ZnS* nanocrystals, the surfactant concentrations 0.25% and 2% were explored, since most of them remained clustered at the interface (as described in the section 5.3) only some droplets showed fluorescence. While in the case of particles, only the surfactant concentration of 2% was explored. At first, the particles accumulated at the interface, but after a few days a small quantity of fluorescent droplets were observed, so we assumed that some particles were encapsulated in the droplets.
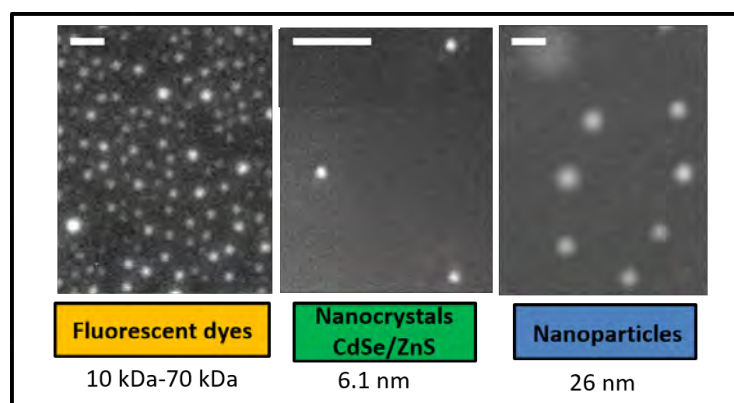
Figure 5.3: Through SE it is possible to encapsulate probe fluorescent species with sizes down to a few *nm*. Scale bar in each figure represents $10\,\mu m$.

It is important to mention that this study was from a qualitative point of view, evaluating whether or not the species in question crossed the interface. In the case of fluorescent dyes (dextran rodhamine $10\,kDa$, $70KDa$ and dextran fluorescein $40KDa$), they pass through the interface without presenting visible accumulations at the interface. The encapsulation process of florescent dyes reminds the passive transport in the cell membrane of living cells, which depends on the polarity and size of the transported molecule [112].

On the other hand, in the case of *CdSe/ZnS* nanocrystals and nanoparticles there is additional phenomena that need to be considered: the nano colloids self-assembly at interfaces. Possibly, the aggregates that form at the interface, being larger than the individual species, do not easily cross the interface. So not all the droplets that are formed contain the probe species (fig. 5.3). The nanometric colloids aggregates can pass the interface after a few days may be due to the fact that the available surfactant at the interface is less and less (because several water droplets have already been generated by SE) and the Span 80 molecules could change their configuration so that large aggrega-

tes could pass through the interface or perhaps some mechanical disturbance caused by handling the cell facilitated the encapsulation of the aggregates.

Also, it would be interesting to explore in more detail the different concentrations of surfactant in all cases and try to find a relationship between the droplets' size, the fluorescent species and the encapsulation capacity of the droplets.

5.3 EVALUATION OF ENCAPSULATION IN SE

In contrast with the case of molecular species in aqueous phase, the majority of nanometric ones remain at the interface (fig. 5.4a) and not inside of the droplets formed by SE. In the literature, there are a lot of works that mention the phenomenon of self-assembly at liquid-liquid interfaces for nanometric species. This particular behaviour is because the interactions (due to shape, wetting properties, charge, etc.) between the colloidal particles at interfaces are different from those in bulk. In addition, for immiscible liquids it is attributed that the high interfacial energy between them can be decreased by the assembly of nanoparticles at the interface [113].
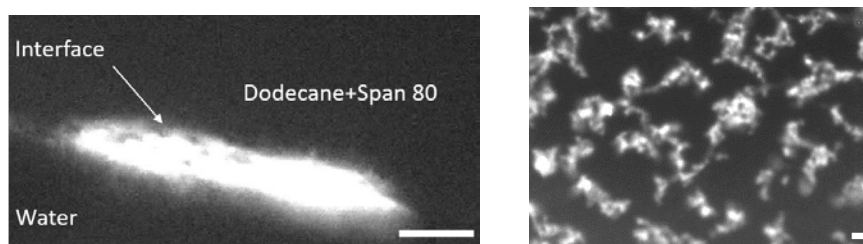
(a) Fluorescence microscopy at the interface between water+nanoparticles and dodecane+span 80. Scale line length $10\,\mu m$.

(b) Aggregated nanocrystals $CdSe/ZnS$ near the interface. Scale bar $1\,\mu m$.

Figure 5.4: The probe species in nanometer range size have a special behaviour near the interface which interferes with our study of encapsulation in SE.

As is shown in fig. 5.4b the nanocrystals $CdSe/ZnS$ form aggregates near the interface between water and dodecane/span 80. Thus, because the aggregates size is large, the droplets formed by SE cannot encapsulate immediately the fluorescent species. The permanence of aggregate particles at the interface between water/oil is also reported for systems such as water/toluene [114].

In the case of nanoparticles, after approximately 12 days, bright droplets are observed in the oil phase, so we assume the nanoparticles cross the interface and are encapsulated by the water droplets. While for the nanocrystals *CdSe/ZnS* this process took approximately four days, but only a few bright droplets are observed.

5.4 DROPLETS SELF-ASSEMBLY IN THE OUT OF EQUILIBRIUM SYSTEM
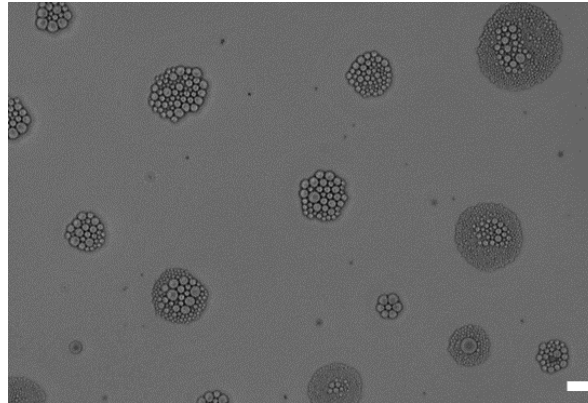
(a) Structures formed by self-assembly in the spontaneous emulsification process after four days from the experiment beginning.
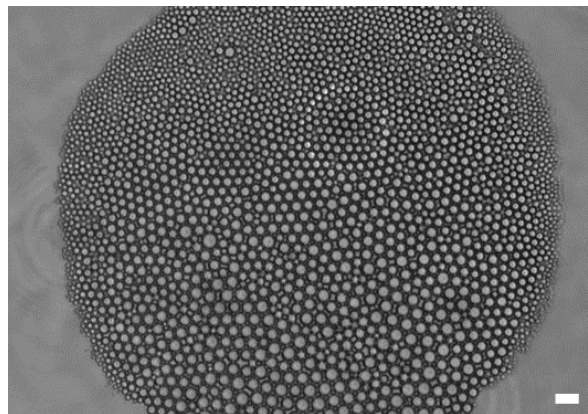
(b) Same experiment of fig. 5.5a after ten days from the experiment beginning.

Figure 5.5: Droplets self-assembled into different structures in the horizontal cell. Scale bar 5 μm.

Another interesting result in horizontal cell is the self-assembly of oil droplets in the aqueous phase as we will explain below. At the beginning of the experiment, we took care about not mixing the liquids. But as soon as the liquids are together, some instabilities appears at the interface. Maybe due the Marangoni effect caused by the

surfactant gradient [115]. This instabilities caused the interface shift towards the dodecane. So we assume, dodecane residues remain on the side of the aqueous phase and dodecane droplets are formed in water. The inverse droplets are in the vicinity of the interface (approximately $150\,\mu m$). Most of the droplets did not show Brownian motion. Except for the smallest ones ($d < 1\mu m$), which are known as satellite droplets [116] because they move around the larger ones (with diameters between $1 < d < 10\,\mu m$). The droplets cluster together forming circular structures, where commonly, larger droplets are in the inner part (fig. 5.5a). After a few days, those structures converge into a larger one (fig. 5.5b). In some cases, a crystalline structure was formed close to the interface, in the aqueous phase formed by a monolayer of hexagonal-packed droplets arranged parallel to the interface, as described in subsection 4.2.1.

The self-assembly of droplets in $2D$ and $3D$ structures was reported in the context of microfluidic chanels [117], [118], clusters formation inside of bigger droplets [119] and with DNA bonds guiding the droplets assembly [120]. The mechanisms used to assemble droplets including for example photo-chemopropulsion [121] by induced chemistry gradients or directional pumping on slippery surface [122]. There is also a report of a gel network structure from purely liquid emulsion droplets [123]. Similar to this case, in the self-assembly in horizontal cell, the adhesion responsible for the random structures formed without coalescence, remains as open question.

The mechanism by which the droplets come together is a sudden movement followed by periods of rest. We do not know the origin of this movement, but it has been reported the droplets generated by SE present concentration gradients that can be enough to drive a droplet to oscillate or jump [124]. In fig. 5.6a we observe examples of metastable states in the droplets self-assembly numbered as I to VII in three minutes interval. I-IV were taken at 91 minutes after the beginning of the experiment, while V-VII were taken at 94 minutes after the beginning of the experiment. The self-assembling droplets are the same during the interval, to recognize each one we numbered them as $1 - 5$. So that, the droplets that was separate in I and IV end up together as it is show in VII. On the other hand, the fig. 5.6b shows the trajectories from the V to VII state. The trajectories are straight lines, like the droplets suddenly slide from the initial position to the final one. The assembly process is not continuous in time but experiences stops and goes. That is, there were moments in which the droplets moved to form aggregates and other intervals in which there
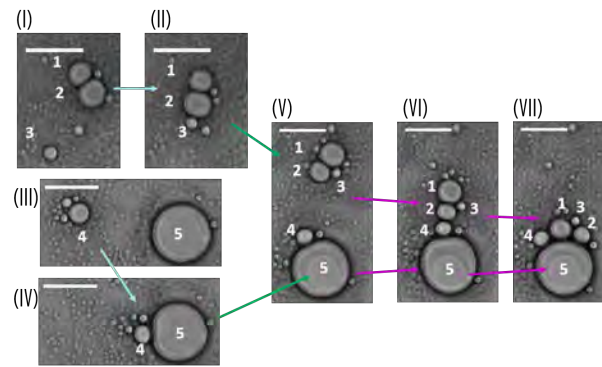
(a) Example of structures formed by self-assembly in the interval of $91 - 94$ minutes after the experiment began.
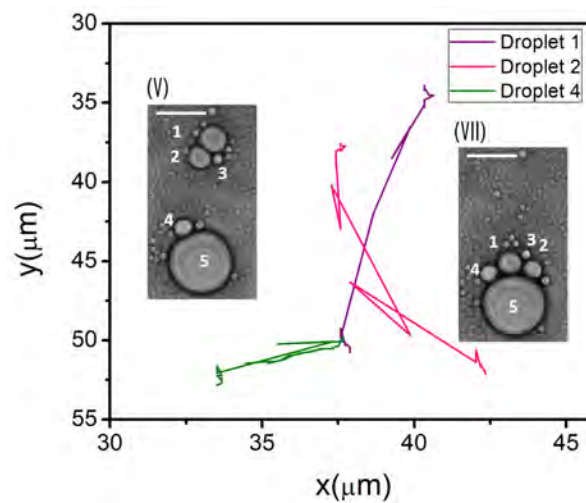

(b) Trajectories of droplets numbered as 1, 2 and 4 in the change to the metastable states V to VII.

Figure 5.6: Droplets self-assembly process is a sequence of metastable states. Scale bar is $10\,\mu m$.

was simply no change. But the final structures were similar in all the experiments.

The droplets velocity is different and the tendency is the biggest droplets come together without coalescence. We tried to estimate some velocities at which the droplets were collecting. Considering displacements in the same direction, the distance between the initial and final points of the droplet was calculated, and the velocity was calculated considering the displacement time. The camera frame rate ($30\,fps$) is not enough to capture the droplets dynamics. For this reason we use the filter *bob doubler* in software *Virtual Dub* to obtain samples an interlaced video at double frame rate ($60\,fps$). In the examples showed in fig. 5.6a the velocities of each droplet are $v_1 = 1.8$, $v_2 = 5$,

$v_3 = 6$ and $v_4 = 70.9\,\mu m/s$ while for fig. 5.6b the velocities are $v_1 = 31.5$, $v_{2.1} = 26.6$, $v_{2.2} = 56.1$ (we split the velocities because there are two segments with different direction in the same trajectory), $v_3 = 22.5\,\mu m/s$.
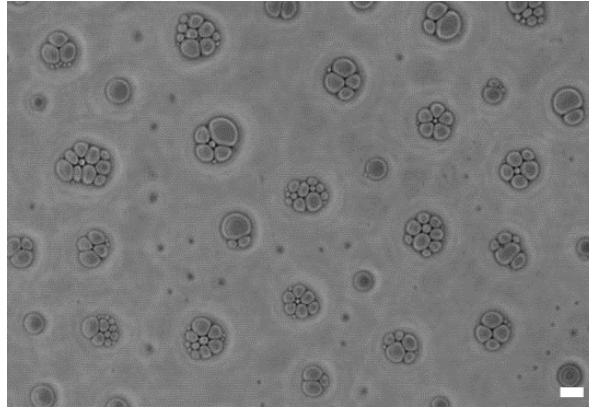
(a) Transmission microscopy of droplets aggregates.
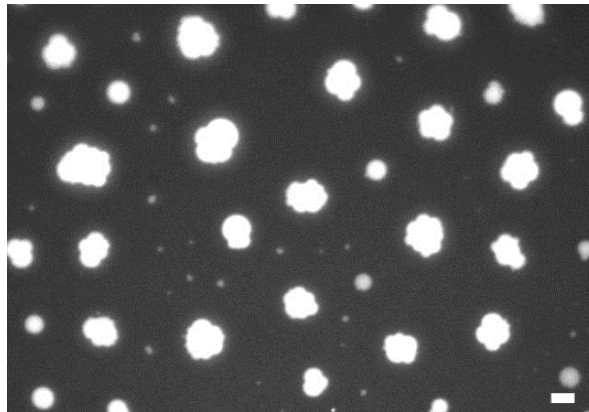
(b) Fluorescence microscopy of droplets aggregates.

Figure 5.7: Droplets self-assembled when we add rhodamine in the oil phase. Scale bar is $5\,\mu m$.

Furthermore, when we added rhodamine B in the oil phase instead of in the aqueous phase, we observed the formation of little different structures in the water phase (fig. 5.7a) that are bright (fig. 5.7b) even though the Rhodamine B was poorly soluble in dodecane. Maybe the rhodamine B act as a co-surfactant in the inverse emulsion oil in water like in the water in oil emulsions stabilized with particles reported in the literature [125]. In emulsion stabilized with Rhodamine B it has been observed that the fluorescent dye confers attraction between the droplets (but the droplets can be separated by gently shaking). Regarding the type of structures formed, we see the individual droplets do not retain their sphericity and the aggregates' shape are reminis-

cent of bubbles clusters or droplet interface bilayers (DIB's) [116].

As we have described, a variety of structures were obtained as a result of self-assembly in the out-of-equilibrium system. It would be interesting to vary parameters such as the concentration of the dye and the surfactant to observe any change and try to establish the parameters in which it is certain that droplets self-assembly occurs. Here we show the qualitative results of these experiments and lay the foundations for possible future work.

REFERENCES

[108] N. Anton and T. F. Vandamme, "The universality of low energy nano emulsification," *International Journal of Pharmaceutics*, vol. 377, no. 1-2, pp. 142–147, 2009 (cit. on p. 51).

[109] M. Guttoff, A. H. Saberi, and D. J. McClements, "Formation of vitamin D nanoemulsion-based delivery systems by spontaneous emulsification: Factors affecting particle size and stability," *Food Chemistry*, vol. 171, pp. 117–122, 2015 (cit. on p. 51).

[110] A. H. Saberi, Y. Fang, and D. J. McClements, "Fabrication of vitamin E-enriched nanoemulsions: Factors affecting particle size using spontaneous emulsification," *Journal of Colloid and Interface Science*, vol. 391, pp. 95–102, 2013 (cit. on p. 51).

[111] K.-M. Park, M.-K. Lee, K.-J. Hwang, and C.-K. Kim, "Phospholipid-based microemulsions of flurbiprofen by the spontaneous emulsification process," *International journal of pharmaceutics*, vol. 183, no. 2, pp. 145–154, 1999 (cit. on p. 51).

[112] N. J. Yang and M. J. Hinner, "Getting across the cell membrane: An overview for small molecules, peptides, and proteins," in *Site-Specific Protein Labeling: Methods and Protocols*, A. Gautier and M. J. Hinner, Eds. New York, NY: Springer New York, 2015, pp. 29–53 (cit. on p. 55).

[113] W. H. Binder, "Supramolecular assembly of nanoparticles at liquid–liquid interfaces," *Angewandte Chemie International Edition*, vol. 44, no. 33, pp. 5172–5175, 2005 (cit. on p. 56).

[114] H. Duan, D. Wang, D. G. Kurth, and H. Möhwald, "Directing self-assembly of nanoparticles at water/oil interfaces," *Angewandte Chemie International Edition*, vol. 43, no. 42, pp. 5639–5642, 2004 (cit. on p. 56).

[115] M. Kullappan and M. K. Chaudhury, "Thermodynamic and kinetic pathways to agitated and spontaneous emulsification," *Langmuir*, vol. 36, no. 34, pp. 10 218–10 237, 2020 (cit. on p. 58).

[116] P. Mruetusatorn, J. B. Boreyko, G. A. Venkatesan, S. A. Sarles, D. G. Hayes, and C. P. Collier, "Dynamic morphologies of microscale droplet interface bilayers," *Soft Matter*, vol. 10, no. 15, pp. 2530–2538, 2014 (cit. on pp. 58, 61).

[117] P. Parthiban, P. S. Doyle, and M. Hashimoto, "Self-assembly of droplets in three-dimensional microchannels," *Soft Matter*, vol. 15, no. 21, pp. 4244–4254, 2019 (cit. on p. 58).

[118] S. Fujiwara, K. Shoji, C. Watanabe, R. Kawano, and M. Yanagisawa, "Microfluidic formation of honeycomb-patterned droplets bounded by interface bilayers via bimodal molecular adsorption," *Micromachines*, vol. 11, no. 7, p. 701, 2020 (cit. on p. 58).

[119] J. Guzowski and P. Garstecki, "Droplet clusters: Exploring the phase space of soft mesoscale atoms," *Physical Review Letters*, vol. 114, no. 18, p. 188 302, 2015 (cit. on p. 58).

[120] L. Feng, L.-L. Pontani, R. Dreyfus, P. Chaikin, and J. Brujic, "Specificity, flexibility and valence of DNA bonds guide emulsion architecture," *Soft Matter*, vol. 9, no. 41, pp. 9816–9823, 2013 (cit. on p. 58).

[121] L. Florea, K. Wagner, P. Wagner, *et al.*, "Photo-chemopropulsion–light-stimulated movement of microdroplets," *Advanced Materials*, vol. 26, no. 43, pp. 7339–7345, 2014 (cit. on p. 58).

[122] J. Jiang, J. Gao, H. Zhang, *et al.*, "Directional pumping of water and oil microdroplets on slippery surface," *Proceedings of the National Academy of Sciences*, vol. 116, no. 7, pp. 2482–2487, 2019 (cit. on p. 58).

[123] J Bibette, T. Mason, H. Gang, and D. Weitz, "Kinetically induced ordering in gelation of emulsions," *Physical Review Letters*, vol. 69, no. 6, p. 981, 1992 (cit. on p. 58).

[124] G. F. Arends, J. M. Shaw, and X. Zhang, "How fast do microdroplets generated during liquid–liquid phase separation move in a confined 2D space?" *Energy & Fuels*, vol. 35, no. 14, pp. 11 257–11 270, 2021 (cit. on p. 58).

[125] J. H. Thijssen, A. B. Schofield, and P. S. Clegg, "How do (fluorescent) surfactants affect particle-stabilized emulsions?" *Soft Matter*, vol. 7, no. 18, pp. 7965–7968, 2011 (cit. on p. 60).

6

CONCLUSIONS AND PERSPECTIVES

The work presented here is not focused on resolving the origin of spontaneous emulsification processes or the attachment of the droplets to the interface, and its connection to the water reservoir, quite interesting by themselves, but one has to device different kind of experiments for such purpose. Here, we report a study on the dynamics of colloidal species in an out-of-equilibrium-system.

The system consisted of an interface between water and oil where water droplets are generated by spontaneous emulsification, i.e. water droplets appear at the interface without supply external energy to the system. The interface had a spherical-like shape and appeared when putting water+glycerol on dodecane+span 80. The water droplets move from the upper to the lower meniscus part, where sediment and form a crystalline structure. The peculiarity of the system is that the droplets move attached to the interface while still growing from submicron sizes to a few microns.

Although the process is complex, the reported phenomenon is qualitatively accurately replicated in a variety of experimental conditions. Remarkably, the movement of individual droplets can be effectively described by a superposition of a normal random process and a constant drift velocity that operates intermittently, i.e. is constant in different periods of time. The statistical properties of the random component match with those of the so called Brownian motion, as demonstrated here and as it occurs in simple fluids in thermal equilibrium. The results suggests that normal diffusion should be expected even in non-equilibrium conditions, and any deviations from normal diffusion may be attributed to other complexities within the system. In this particular case, the deviations are caused by the presence of a drift velocity. The cause of the droplets' drift in their motion could be attributed to the effect of gravity not only on the droplets but also mainly on the interface, which generates a very low downstream movement that carries the droplets along.

On the other hand, related with the complexity of the process, we observe changes in the droplets behaviour during the experiment evolution in time, such as the number of droplets decrease as well as

the average velocity in the direction toward the CS. We associate the changes to the dynamical properties of the interface. In addition, we observe other structures product of self-assembly when we modify the confinement of the interface and adding a new parameter, the presence of dye in aqueous phase.

Returning to the idea of the introduction of this thesis, and continuing with the beauty of the methodological process in research, we obtain answers and also more questions. Exploring the concentration of glycerol that would be added to the aqueous phase, limit concentrations were found in which the drift due to gravity in the droplets movement seemed to disappear and as the glycerol concentration decreased, the drift was observed again. So, it would be interesting to analyse the droplets behaviour by varying the glycerol concentration parameter. In addition, one can continue working, trying to understand the self-assembly process in horizontal cell, varying the dye concentration and exploring if there is a limit case where the self-assembly doesn't occur. In drawing things to a close, spontaneous emulsification is a very interesting topic as an out-of-equilibrium-process, and also as a system to modelling diffusion in this kind of systems.

Part II

APPENDIX

DESCRIPTION OF THE METHODOLOGY DETAILS

A.1 APPROXIMATION TO THE GEOMETRIC SHAPE OF THE CAPILLARY MENISCUS

The cell's geometry, described in the previous section, where the two aqueous fluid phases meet a solid phase leads to the formation of a capillary convex meniscus. This is due to the competence between liquids surface energies. On the other hand, in small capillaries (radius r), as we assume in our case, can be considered that a capillary meniscus forms part of a sphere and the curvature at the three-phase contact line is reduced by [126],

$$R_{sph} = \frac{r}{cos\theta},$$ (A.1)

and for a small enough capillaries the maximum depth is,

$$h = R_{sph}\left(1 - sin\theta\right),$$ (A.2)

On the other hand, Cheong and co-workers [127], considering spherical shape of the meniscus, showed that knowing the capillary radius and height of the meniscus, i.e. the meniscus' shape, is enough to calculate the contact angle, as follows:

$$\theta = tan^{-1}\left(\frac{r^2 - h^2}{2rh}\right),$$ (A.3)

Experimentally, we know the capillary radius r_{cell} (figure A.1): we take microscopy images of all of the empty cells and then measure the radius with the circle feature measure tool include in the Image Pro Plus program. In addition, we are able to measure the height of the meniscus (h) once the crystal structure (CS) covered all the interface. In this fashion, approximately after three hours from the beginning of the experiment, we can identify the CS center that in the best scenario correspond with the meniscus lowest part and the end matches to the meniscus highest part. Namely, through focusing the droplets in both regions with the adjustment knob and identifying the height with the
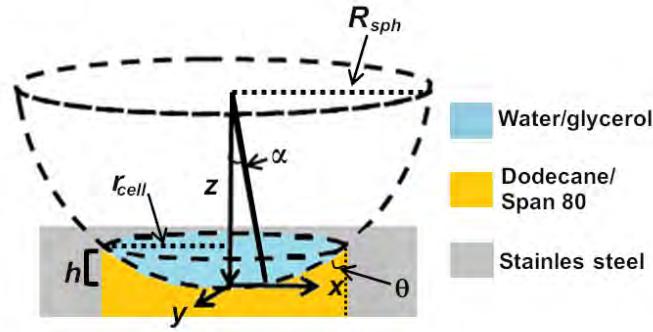
Figure A.1: Side view of the sample cell with the geometrical considerations made to describe the interface as a spherical surface cap.

scale in microns. The heigh measures were made in four different ends (separately 90°) and the values were averaged. With the values of h, r_{cell} and assuming a spherical shape interface we calculated the contact angle and the radius of the sphere using eq. A.3 and eq. A.2 respectively.

In different realizations of the experiment, there are slight differences between the cells' radii. Thus, the meniscus shape is not exactly the same for all experiments. For comparison purposes, we show three different graphs (figure A.2) of geometry menisci for: $h = 115\,\mu m$, $80\,\mu m$, $60\,\mu m$ with $r_{cell} = 567.48\,\mu m$ for the two first heights and $r_{cell} = 583.27\,\mu m$ for the last one. The two first cell radii values reflects that although we use the same cell, there are differences in the meniscus shape due to the other aspects that influence the meniscus height: such as the quantity of epoxy resin used to seal the cell, since a little bit more epoxy resin (the order of μl) increases the cell height, modifying its volume and therefore the meniscus high. Also, if we put the epoxy resin very close or far from the cell hole, we modify the cell volume and consequently the meniscus height. It's important to mention, that despite all possible differences, the phenomenon is qualitatively well reproducible.

For the sake of clarity, in the menisci shape graphs, we used dimensionless quantities: $\sqrt{x^2 + y^2}/r_{cell}$ where the numerator is the radial coordinate on the Cartesian plane, and z^*/R_{sph} where z^* is the meniscus high measured from the lower part of the meniscus. As observed in figure A.2, the greater the height of the meniscus, the greater the radius of the sphere that contains it.
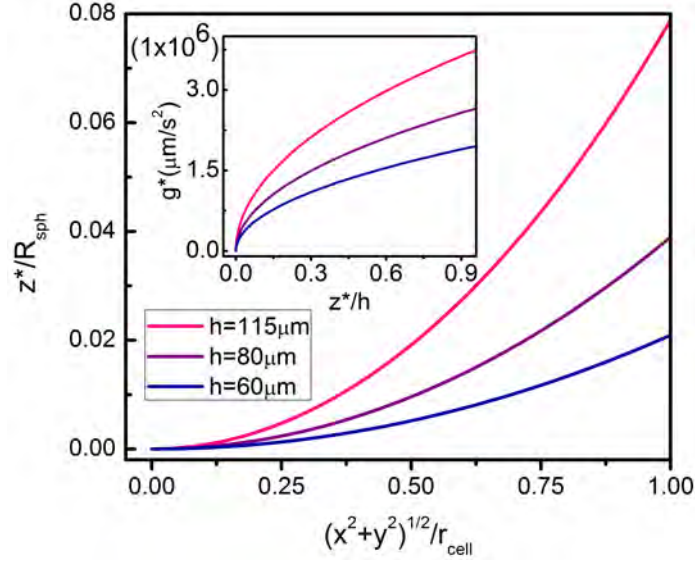
Figure A.2: The meniscus shape depends of the meniscus high and cell radius as well as the gravity value calculated as a function of the meniscus height as showed in the inset.

For the different meniscus obtained in different experiments realizations, the quantities showed in fig. A.1 are: the angle α is about $0.164 - 0.371$ rad, this means that in this area the component of the gravity along the surface is quite small; the meniscus height h is between $50 - 115\,\mu m$ and the radius of sphere that fits to the meniscus shape R_{sph} is about $1457 - 3615\,\mu m$.

A.1.1 *Acceleration due to gravity at the interface*

In order to know the acceleration due to gravity, g, that act at the interface, we need to calculate the angle α showed in the figure A.1. This is the supplementary angle to the latitude angle α^*, where $0 \leq \alpha^* \leq \pi$. We change the common nomenclature so as not to confuse it with the contact angle θ. It is possible to calculate α for any position in the meniscus, assuming that all pair points x, y that we observe in the meniscus microscopy images are on the sphere and $\alpha^* + \alpha = \pi$, as follows:

$$R_{sph} = \sqrt{x^2 + y^2 + z^2} \tag{A.4}$$

From eq. A.4 we can calculate z for any x, y point of interest. Then, from the spherical coordinates, we know that $z = R_{sph} \cos\alpha^*$ with α^* in clockwise direction, so that for the lowest meniscus part $\alpha^* = \pi$.

Particularly, for the highest meniscus part, for the Cartesian point $(r_{cell}, 0)$, we have:

$$\alpha^* = cos^{-1}\left(\frac{sqrt(R_{sph}^2 - r_{cell}^2)}{R_{sph}}\right), \tag{A.5}$$

The meniscus angle value for different experiments was in the range of $0.164 < \alpha < 0.371\ rad$. On the other hand, if we imagine a droplet moving over the interface from the highest to the lowest position of the meniscus, we can establish the gravity contribution that is experienced by the droplet (g^*). This, from a relatively simple approach, from the free body diagram without considering other forces, i.e. $g^* = gsin\alpha$. As shown in the inset in figure A.2, the gravity experienced by a droplet is greater while the greater meniscus height. On average the maximum gravity experienced by a droplet is $g^* = 0.2g$.

A.1.2 *Flat Interface Approach*

Continuing with the interface shape description, regarding the spherical radius the meniscus, R_{sph}, its value is between $1.62 - 3.61\ mm$. Considering $r_{cell} \approx 0.6\ mm$, we have that $2.7r_{cell} < R_{sph} < 6r_{cell}$. However, the droplets move on a spherical surface, shown in fig. A.3 (in gray color is showed part of the sphere and the red line indicates the meniscus height) which can be approximated as a flat surface because $R_{sph} > r_{cell}$. More clearly, from a geometric point of view, for small angles ($sin\beta \approx \beta$), as showed in in the same fig. A.3. If we calculate the arc length, the purple dotted line $s = R\beta$ and compare it with the line length (Δr), in orange color, delimited for the same angle we find that $s \approx \Delta r$. Thus, we can assume that the droplets move on a flat interface since the angle that delimits the meniscus is small and besides the observation region in each experiment is just part of the interface. This assumption is reforced because during the experiments, the droplets move along the observation plane of the analysed region.

A.2 DROPLETS' SIZE

Regarding the droplet's size measurement, two regions can be distinguished in the images: (1)the droplets that occupy a place in the crystalline structure (CS) and (2)the droplets that are moving over the interface towards the CS. The images are cropped to work with each region separately. Because the droplets increase in size over time, only 22 frames ($\approx 1\ s$) are used for each set of measurements, where the
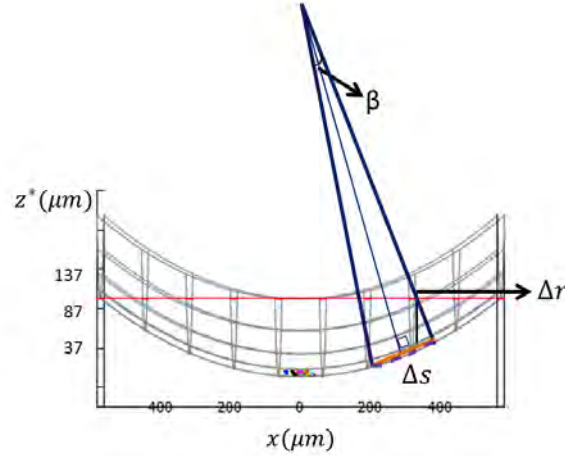
Figure A.3: Although the droplets move over a section of a spherical surface, we can assume it as a flat interface. This is because β in all cases is small.

procedure is repeated and the results averaged.

For the droplets in region (1), using the plugins included in Image J, the droplets centers are first identified and then Voronoi diagram tessellation is used to join them (fig. B.8a). The measurement considered is on the length of these lines, which correspond to the droplets diameter. The only edges that have to be ignore for the calculation are the edges at the boundaries of the crystal since they do not represent real droplet connections.

On the other hand, for the droplets in region 2, we use Image J to identify the regions of maximum intensity, after applying the mask that changes the images to binary type where the droplets are identified in black color and the background in white one (fig. A.4b). The measurements are made on the maximum diameter of the individually-identified dark circular regions. This measurement on average corresponds to the diameter of each droplet.

A.3   TRAJECTORY FRAGMENTATION

Trajectory data mining has become an important research topic, due to the applications in different areas such as geography, biology, sociology and computer science. Trajectories provide information to understand moving objects and their environment and in many scenarios we need to divide trajectories into segments to analyse them more precisely according to the movement type observed. By segmentation

(a) Region 1: droplets in the Crystalline   (b) Region 2: *free*
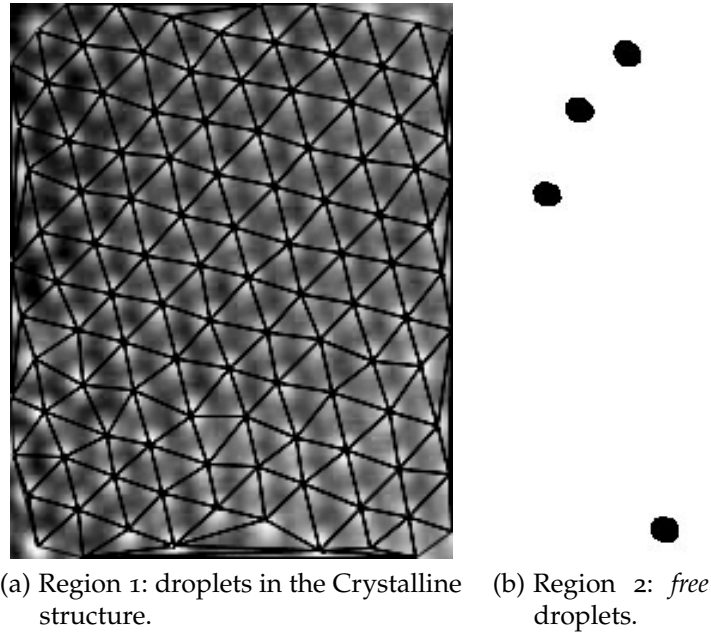   structure.   droplets.

Figure A.4: The size of the droplets is determined according to the region in
            which they are located. For droplets in the crystal structure (CS),
            Voronoi tessellation is used, while for droplets moving towards
            the CS, the maximum diameter of the droplets identified as the
            darkest regions is measured.

we can find sub-trajectory patterns, which allow us to revel details
that we can not extract from an entire trajectory. There are different
ways to do trajectory segmentation, but in general, there are three
types of segmentation methods: time interval, shape of the trajectory
and semantic meaning [128]. In our study system we use the seman-
tic meaning of the positions relative to the CS to stablish the general
classification and a combination of the trajectory shape and the local
property of turning points to segment each one, as we describe below.

Droplets in each experiment were classified according with their po-
sition: crystalline structure (CS), *droplets near* to the CS boundary (in
a distance between the boundary and five droplet's diameters away)
and the rest of droplets classified as far from the CS boundary. The
considered diameter is the droplets in CS one. Some droplets moved
in more than one region of interest, and it was necessary to fragment
their length trajectories according to the established regions. So each
fragment was handled as a new trajectory.

In general, in the literature four basic types of motion are observed
in single particle tracking experiments: normal diffusion, directed mo-
tion, anomalous diffusion, and confined diffusion [129]. According to

the observed trajectories, in our experiment we find two cases: directed motion (droplets moving towards CS) and confined diffusion (droplets near the CS). We specially work with droplets far from the CS boundary, approximately 5 μm from de CS boundary. Every trajectory was analysed, as follows: most of the times the droplets move with constant velocity for variable periods of time. For each change in their movement direction and consequently their velocity, we separate a fragment. This analysis is performed separately for x and y components, helping us with a position vs lag time graph. The procedure consist of drawing a straight line on the graph that fit approximately to the most part of the trajectory. If there is a change in the droplets velocity, then one line is not enough to fit all the trajectory and the point of the direction change designates the start of a new line and as a result a new trajectory. In the figure below, there are two examples: 1) fig.A.5a show the fragmentation of trajectory near the CS boundary (approximately 5 μm from the CS boundary), the characteristic behaviour is that the droplet moves to a site in the CS so the droplets have almost zero velocity in both directions; 2)fig. A.5b show the trajectory of a droplet far from to the crystal boundary, in the y coordinate the velocity is the same for all trajectory while for a x coordinate there are two different velocities along the trajectory due to a slight velocity increase in the final part of the trajectory.

(a) Near droplet trajectory fragmentation.

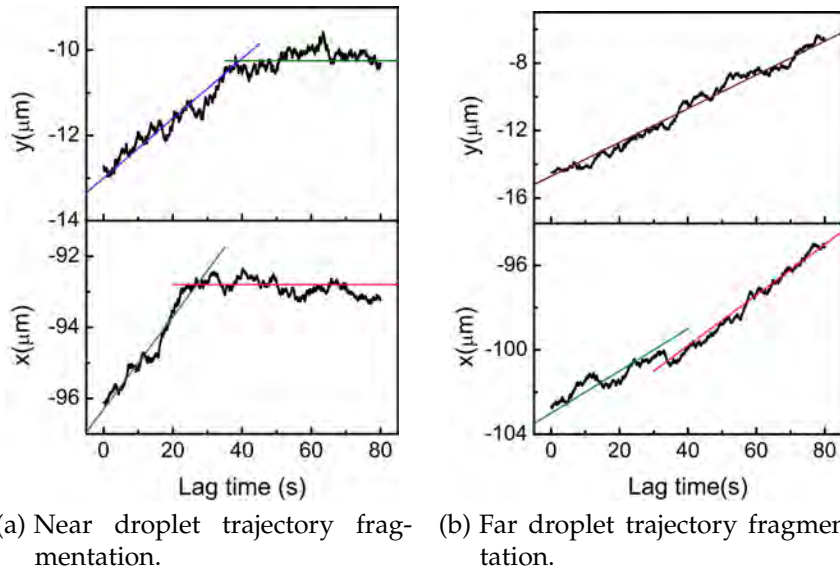(b) Far droplet trajectory fragmentation.

Figure A.5: Each trajectory is unique so, they are fragmented considering their individual behaviours.

Since each trajectory is unique, the fragmentation depends on each one as it is shown in the examples in fig. A.5. After the fragmentation

is done, the analysis is the same for each part of the trajectory. It is found that the droplets have similar behaviour in the region where they move.

Also, it is important to mention that this fragmentation methodology was applied in the analysis of individuals particles trapped in an optical line oriented in the gravity axis and generated by a spatial light modulator. The article is under revision and the work was performed as a collaboration with other members of the complex fluids laboratory [130].

A.4 DROPLET'S VELOCITY

In order to calculate the droplet velocity v we consider: 1)the limit case of a water droplet, radius r_d, falling in oil toward the bottom of the cell, i.e. where the maximum droplet velocity possible is due to gravity and 2)buoyancy, then the Stokes-Einstein relation is used as follows:

$$v = \frac{4g\Delta\rho D_y \pi r_d^3}{3k_B T}, \tag{A.6}$$

where $\Delta\rho$ is the difference in densities between water and dodecane, D_y is the diffusion coefficient of the water droplet in oil and T is the room temperature ($295.15\,K$). Using typical values founded in the experiment, i.e. $r_d = 0.5\,\mu m$ and $D_y = 0.2\,\mu m^2/s$, the velocity is $v \approx 0.003\,\mu m/s$. The smallest velocity observed in the experiments is an order of magnitude higher, so we infer there is a kind of flow at the interface that increases the droplets velocity. We think this flow is due to gravity influence on the interface.

REFERENCES

[126] F. Eslami and J. A. Elliott, "Gibbsian thermodynamic study of capillary meniscus depth," *Scientific Reports*, vol. 9, no. 657, pp. 1–17, 2019 (cit. on p. 66).

[127] B. Huey-Ping Cheong, T. Wah Ng, Y. Yang, and O. Wah Liew, "Using the meniscus in a capillary for small volume contact angle measurement in biochemical applications," *Langmuir*, vol. 27, no. 19, pp. 11 925–11 929, 2011 (cit. on p. 66).

[128] Y. Zheng, "Trajectory data mining: An overview," *ACM Transactions on Intelligent Systems and Technology (TIST)*, vol. 6, no. 3, pp. 1–41, 2015 (cit. on p. 71).

[129] P. Kowalek, H. Loch, and J. Szwabiński, "Classification of diffusion modes in single-particle tracking data: Feature-based versus deep-learning approach," *Physical Review E*, vol. 100, no. 3, p. 032 410, 2019 (cit. on p. 71).

[130] "Quasi-1D sedimentation of brownian particles along optical line traps," *Optics & Laser Technology*, vol. 161, p. 109 212, 2023 (cit. on p. 73).

ADDITIONAL RESULTS

B.1 OTHER EXAMPLE OF SINGLE TRAJECTORY ANALYSIS
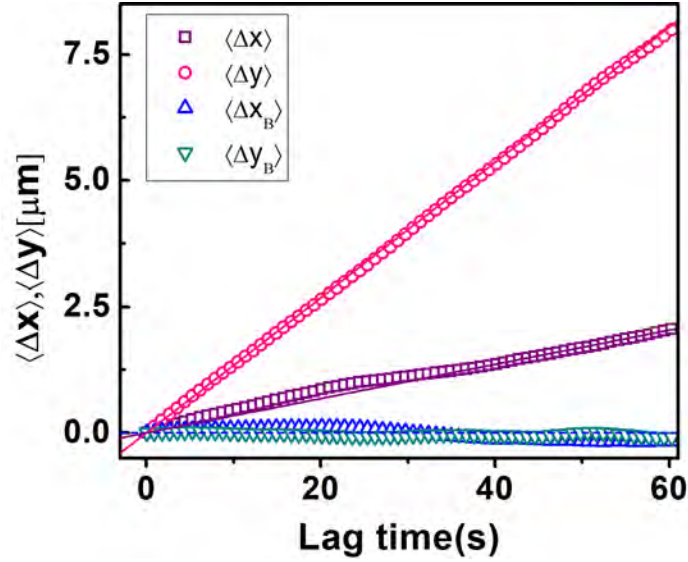
Figure B.1: Droplet's mean displacement, total (squares and circles) and Brownian (diamonds and triangles) along directions x and y, respectively.

As we mention in subsection 4.4.1, here we show the analysis of other trajectory in fig. 4.8b, the one marked with a double asterisk. For the trajectory analysed in this part, it is found from the fits that $v_x = 0.03 \mu m/s$, $v_y = 0.134 \mu m/s$, $D_x = 2.3 \times 10^{-2} \mu m^2/s$ and $D_y = 1.8 \times 10^{-2} \mu m^2/s$. The velocity is small for x direction because the motion of the droplet is almost straight towards the CS (fig. B.1). In fig. B.2 the experimental distribution functions of steps at three different times $t = 1, 10, 60\Delta t$ (open symbols) are presented. Again the shape and symmetry of these functions coincide with the distribution function of steps x for a single particle, diffusing with a diffusion constant D in a fluid in thermal equilibrium, given by the Gaussian function. The value of D used here is the average of D_x and D_y.

The fitted values for the velocity and diffusion constant can be input in eq. 4.5 to compute the mean square displacement and compare it with the experimental results. As shown in fig. B.3 the agreement between experiment (open symbols) and eq. 4.5 (lines) is quite remar-
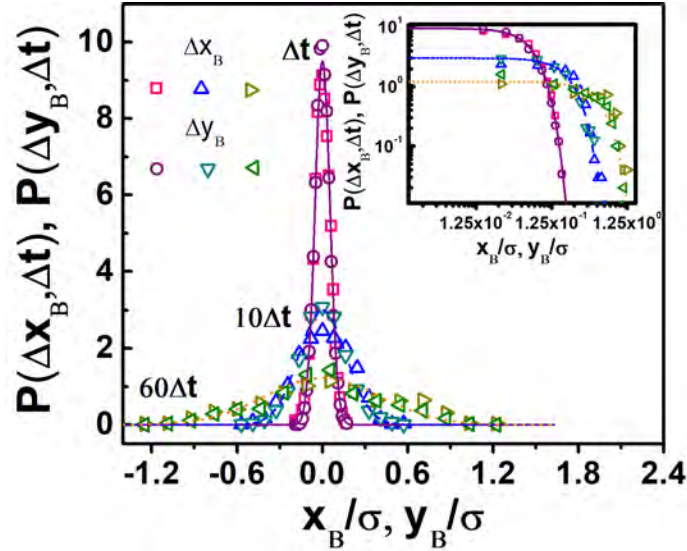
Figure B.2: Step distribution functions of the Brownian displacements at three times, experimental (symbols) and Eq. 4.6 (lines). The inset shows the data of the distribution function only for positive displacements in log-log scale.

kable for a wide range of time. In this trajectory D_x and D_y are slightly different, as we can see at short times, while v_x and v_y are different, so the graphs differ at longer times. The distribution function, at three times, $P_G(x + vt, t)$ is shown in fig. B.4, the open symbols are experimental data and lines are the fitting to eq. 4.6 for the variable $x + vt$.

Finally, as in the subsection 4.4.1, in fig. B.5 is shown the agreement between the fitting to eq. 4.8 and the previous values obtained from the fitting to eq. 4.6.

B.2 CRYSTAL STRUCTURE GROWTH

When we observed the interface with the Thorlabs camera, we were not able to distinguish the CS complete formation. In order to obtain the total interface view, we used another camera with a smaller pixel size. Sacrificing the detail observation, we were able to observe the complete structure growth. Time lapse pictures are shown in fig. B.6, which were obtained with a Hamamatsu Camera $C9100 - 14$ in five minutes intervals. These pictures show the CS circular shape imposed by the stainless steel cell that is maintained while the structure grows. This is due because the boundary conditions dominate the CS structure, as it is described by Bubeck and co-workers [131].
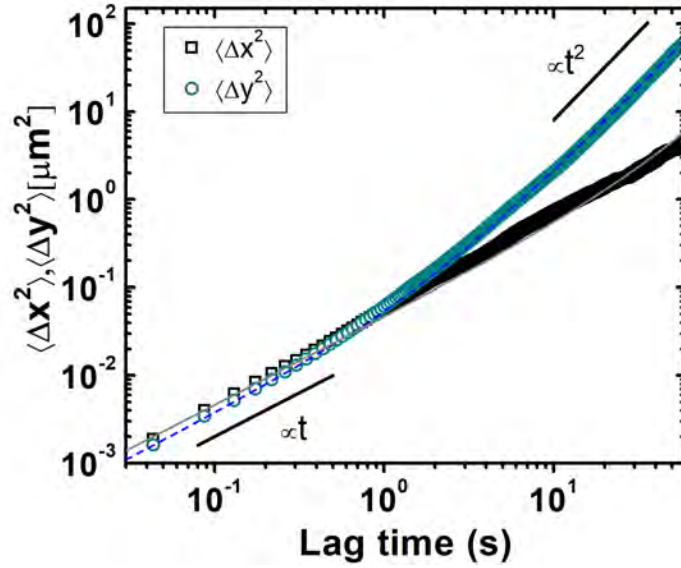
Figure B.3: Mean squared displacement along x and y directions (symbols) correspond to the experimental results and lines are Eq. 4.5 using the fitting values for velocity components and diffusion constant obtained from the data in fig. B.1 and B.2, respectively.

B.3 AREA FRACTION IN CS FORMATION STAGES

It is supposed the droplets arrive to the CS in a similar way from any direction. In order to describe the CS formation we established three different stages based on the number of observed droplets that approach to the CS structure on a chosen square area within the observation field of view, $A_{region} = 2125\,\mu m^2$. The calculation of the area fraction, ϕ, was performed in terms of:

$$\phi = \frac{A_{droplets}}{A_{region}}, \tag{B.1}$$

where $A_{droplets}$ is the area of all droplets observed in the square region, localized at least $5\,\mu m$ to the CS border. The Image J program was used to make the measurements. First a square region was selected, and then separated from the rest of the image. Second, in that image, the number of droplets was identified, and their area is calculated. Finally, ϕ is obtained with eq. B.1 and the previous values.

We identified the area fraction values of the droplets that approaching the CS to be between $0.3 > \phi > 0$. The number of new droplets moving over the interface decreases as a function of time, in such a way that fraction area, ϕ, decreases since the start of the experiment
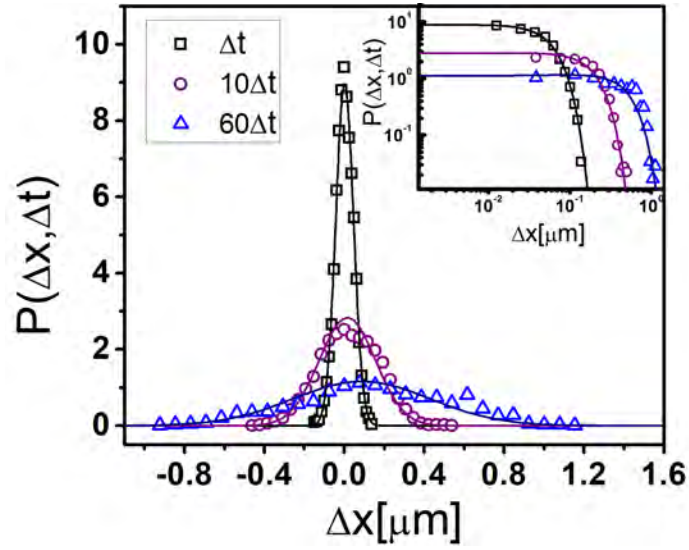
(a) Step distribution function along *x* direction.
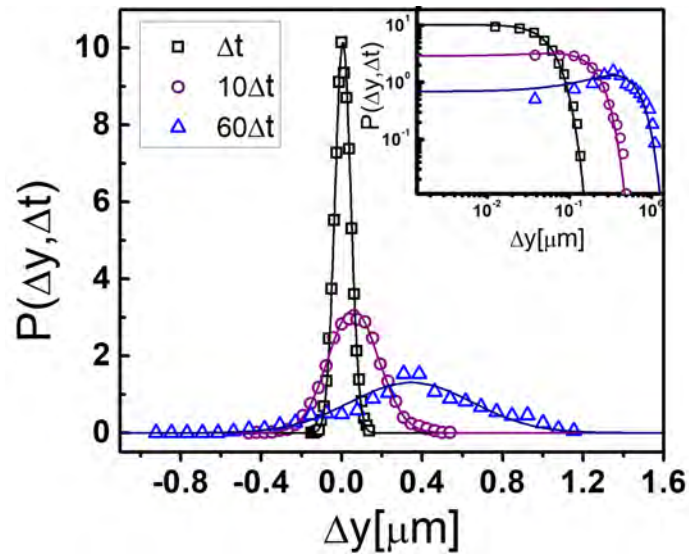
(b) Step distribution function along *y* direction.

Figure B.4: The step distribution function along *x* and *y* direction at three different times, obtained experimentally (symbols) and from Eq. 4.6 (lines). The inset shows the data of the distribution function only for the positive displacements in the log-log scale.
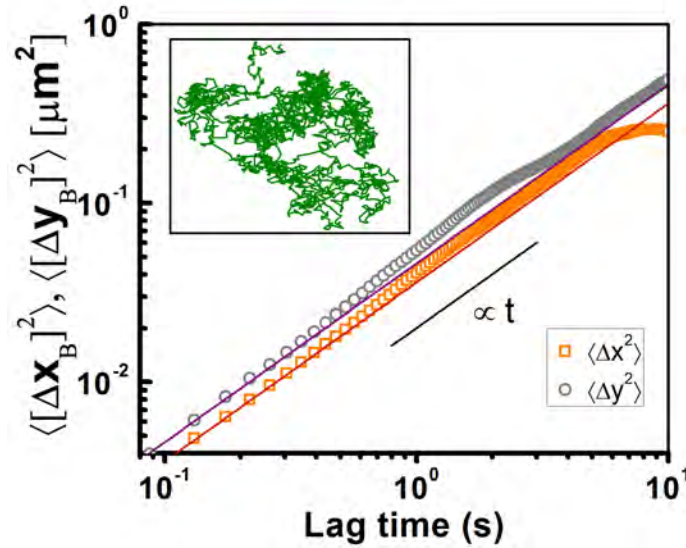
Figure B.5: Mean squared displacement along x and y directions (symbols) correspond to the experimental results and lines are eq. 4.8 fitting, by which the diffusion constant is obtained. We observe a good agreement with the previous calculated values. The inset is the experimental trajectory obtained after eq. 4.7.

until the end. Taking into account this decrease in ϕ is how we defined the stages of CS formation, as is described in chapter 4. For the sake of clarity, illustrative images of droplets approaching to the CS structure from one experiment and their corresponding area fraction values are shown in fig. B.7. Around 60 minutes there is a change in ϕ. This decrease in the number of droplets approaching to the CS border define the limit between two different stages: intermediate and final.

B.4 ORDER IN CRYSTALLINE STRUCTURE

As already mentioned in section 3.2, particles at a liquid interface clump together as a result of capillary attraction. In this case, the constant-contact angle condition along the contact three-phase line can only be satisfied when the interface is deformed [132]. In addition, self-assembly is a robust and easy way to obtain ordered colloidal 2D structures. However, because of uncontrolled nucleation and growth, most of the structures formed by this mechanism exhibit a disorder degree for instance, grain boundaries and point defects [133]. Once the droplets cover the entire interface and the experiment is considered to be over, some images of the crystal structure are taken. These images were analysed in Image J by means of Voronoi triangulation.
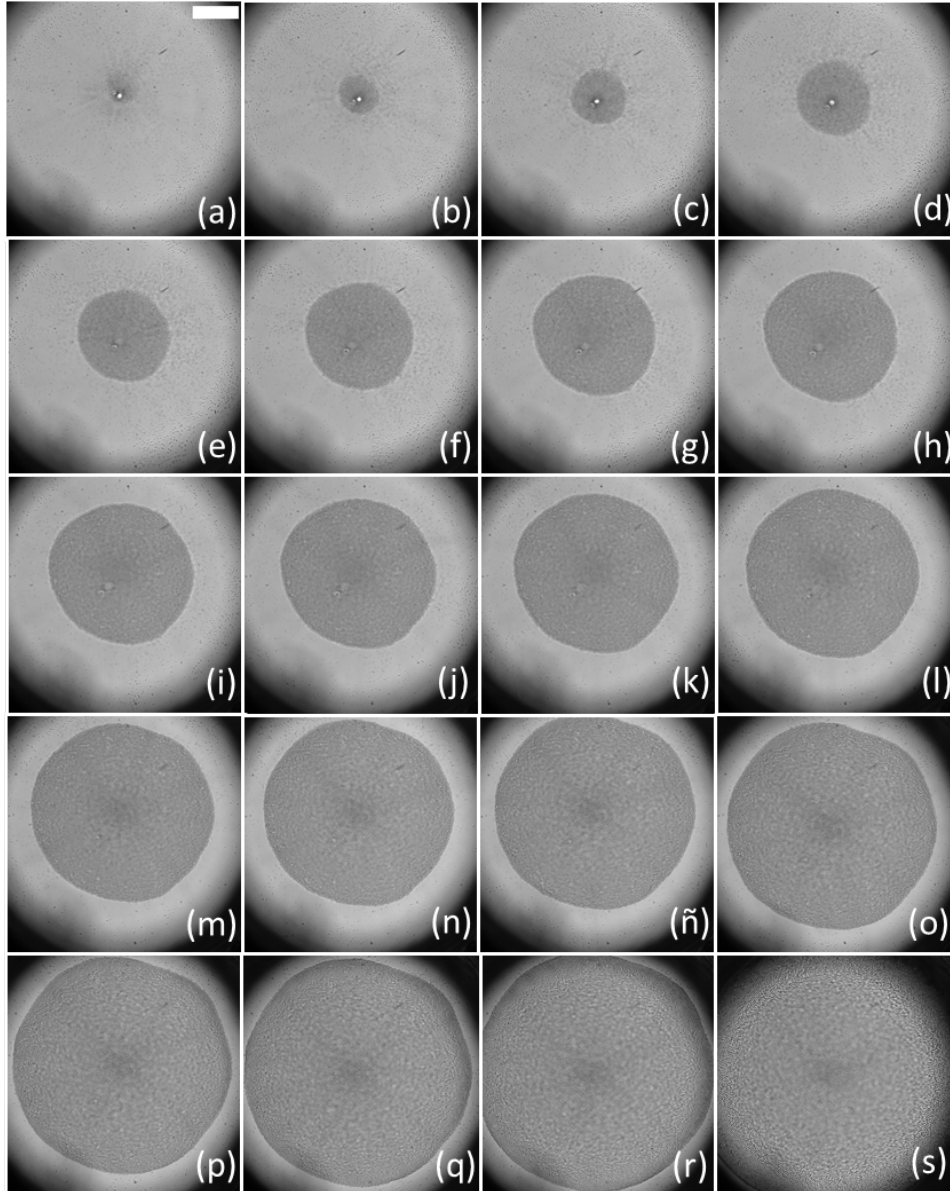
Figure B.6: CS evolution in time: (a)25, (b)30, (c)35, (d)40, (e)45, (f)50, (g)55, (h) 60, (i)65, (j)70, (k)75, (l)80, (m)85, (n)90, (ñ)95, (o)100, (p)105, (q)110, (r)115, (s)135 minutes. The scale bar is 150 μm.
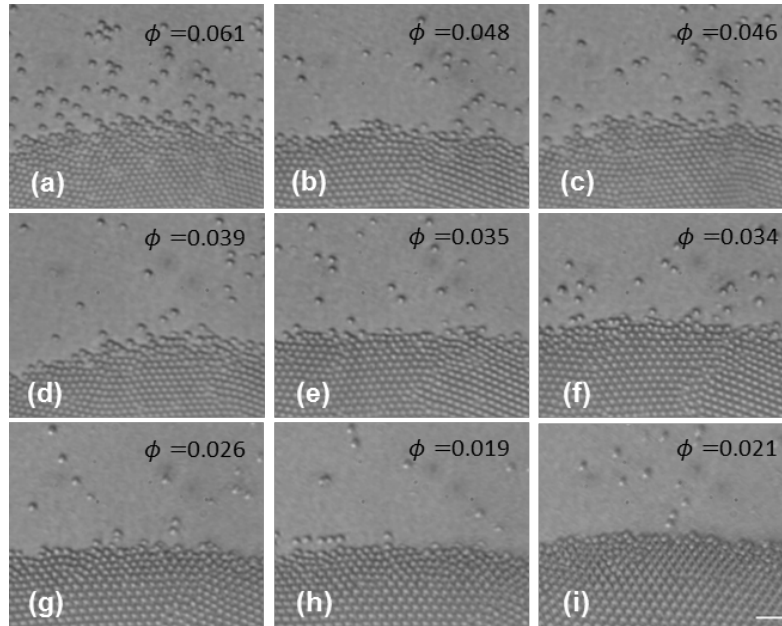
Figure B.7: As an example, it is shown image sequence for the calculation of ϕ at different times: (a)47, (b)50, (c)55, (d)57, (e)66, (f)71, (g)75, (h)79, (i)84 minutes. The scale bar is the same for all sub-pictures 10 μm.

As described by Pertsinidis and co-workers [134], in order to characterize the configuration of the defects it is necessary to identify the poorly coordinated particles, i.e. the ones that don't have six neighbours. The elastic model of Bausch et al [135] showed that a single isolated 5-sided declination would cause a large local strain, resulting in a large elastic energy penalty. To avoid the penalty, the CS creates defects chains that gradually reduce the tension. The chain belong to the system in thermal and mechanical equilibrium and consist of pairs of point defects of droplets with coordination numbers 5(red points) - 7 (yellow points) aligned consecutively, as shown in fig. B.8a.

Locally the order is preserve, but not in globally way. The experimental observations of the crystalline structures allowed the identification of some defects associated with vacancies. Two main types of point defects [136] were found: associated with monovacancy and divacancy (fig. B.8b). From top to the bottom part and from left to the right: split, threefold symmetric, twofold crushed, split due to divacancy and the last examples of vacancies in CS.

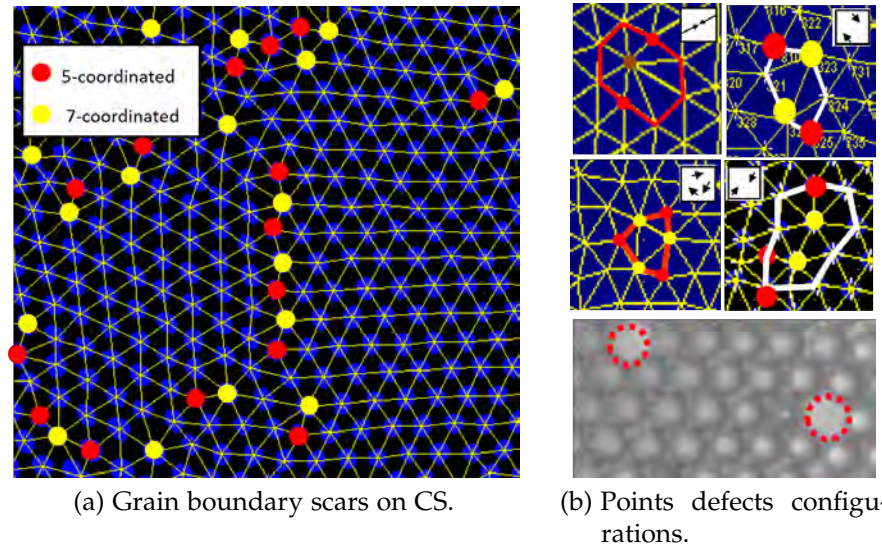(a) Grain boundary scars on CS.

(b) Points defects configurations.

Figure B.8: Long-range crystalline order and interface curvature are incompatible. Thus, the crystalline structure presents point defects that are grouped in grain boundary scars.

REFERENCES

[131] R. Bubeck, S. Neser, C. Bechinger, and P. Leiderer, "Structure and dynamics of two-dimensional colloidal crystals in confined geometry," *Trends in Colloid and Interface Science XII*, pp. 41–45, 1998 (cit. on p. 76).

[132] D. Ershov, J. Sprakel, J. Appel, M. A. Cohen Stuart, and J. van der Gucht, "Capillarity-induced ordering of spherical colloids on an interface with anisotropic curvature," *Proceedings of the National Academy of Sciences*, vol. 110, no. 23, pp. 9220–9224, 2013 (cit. on p. 79).

[133] Q.-H. Wei, D. Cupid, and X. Wu, "Controlled assembly of two-dimensional colloidal crystals," *Applied Physics Letters*, vol. 77, no. 11, pp. 1641–1643, 2000 (cit. on p. 79).

[134] A. Pertsinidis and X. Ling, "Equilibrium configurations and energetics of point defects in two-dimensional colloidal crystals," *Physical Review Letters*, vol. 87, no. 9, p. 098 303, 2001 (cit. on p. 81).

[135] G. Meng, J. Paulose, D. R. Nelson, and V. N. Manoharan, "Elastic instability of a crystal growing on a curved surface," *Science*, vol. 343, no. 6171, pp. 634–637, 2014 (cit. on p. 81).

[136]   A. Pertsinidis and X. S. Ling, "Video microscopy and microme-
chanics studies of one-and two-dimensional colloidal crystals,"
New Journal of Physics, vol. 7, no. 1, p. 33, 2005 (cit. on p. 81).

RIGHTS AND PERMISSIONS

Spontaneous Two-Dimensional Spherical Colloidal Structures

Author: Héctor González-Ochoa, José Luis Arauz-Lara
Publication: Langmuir
Publisher: American Chemical Society
Date: May 1, 2007

Copyright © 2007, American Chemical Society

PERMISSION/LICENSE IS GRANTED FOR YOUR ORDER AT NO CHARGE

This type of permission/license, instead of the standard Terms and Conditions, is sent to you because no fee is being charged for your order. Please note the following:

- Permission is granted for your request in both print and electronic formats, and translations.
- If figures and/or tables were requested, they may be adapted or used in part.
- Please print this page for your records and send a copy of it to your publisher/graduate school.
- Appropriate credit for the requested material should be given as follows: "Reprinted (adapted) with permission from {COMPLETE REFERENCE CITATION}. Copyright {YEAR} American Chemical Society." Insert appropriate information in place of the capitalized words.
- One-time permission is granted only for the use specified in your RightsLink request. No additional uses are granted (such as derivative works or other editions). For any uses, please submit a new request.

If credit is given to another source for the material you requested from RightsLink, permission must be obtained from that source.

Figure C.1: Permissions figure 3.2a.

Figure C.2: Permissions (part 1) of figure 3.2b.

Type of Use	reuse in a thesis/dissertation
Portion	figures/tables/illustrations
Number of figures/tables/illustrations	1
Format	both print and electronic
Are you the author of this Elsevier article?	No
Will you be translating?	No
Title	Movement of spontaneously emulsified water droplets on an out-of-equilibrium surface
Institution name	Universidad Autónoma de San Luis Potosí
Expected presentation date	Feb 2023
Portions	Figure 1 (b) optical microscope image

Figure C.3: Permissions (part 2) of figure 3.2b.

APS American Physical Society
Reuse and Permissions License

16-Feb-2023

This license agreement between the American Physical Society ("APS") and Maria de Jesus Martinez-López ("You") consists of your license details and the terms and conditions provided by the American Physical Society and SciPris.

Licensed Content Information

License Number:	RNP/23/FEB/063272
License date:	16-Feb-2023
DOI:	10.1103/PhysRevE.106.034615
Title:	Brownian motion on an out-of-thermal-equilibrium surface
Author:	Maria de Jesús Martinez-López and José Luis Arauz-Lara
Publication:	Physical Review E
Publisher:	American Physical Society
Cost:	USD $ 0.00

Figure C.4: Permissions of figures (part 1) 4.2, 4.8, 4.9, 4.10, 4.11 and 4.12a.

Request Details

Does your reuse require significant modifications: No

Specify intended distribution locations:	México
Reuse Category:	Reuse in a thesis/dissertation
Requestor Type:	Author of requested content
Items for Reuse:	Figures/Tables
Number of Figure/Tables:	4
Figure/Tables Details:	Figure 1 is schematic. Figure 2, 3, 4 are representation of experimental data
Format for Reuse:	Electronic and Print
Total number of print copies:	Up to 1000

Information about New Publication:

University/Publisher:	Universidad Autónoma de San Luis Potosí
Title of dissertation/thesis:	Movement of spontaneously emulsified water droplets on an out-of-equilibrium surface
Author(s):	María de Jesús Martínez-López
Expected completion date:	Feb. 2023

Figure C.5: Permissions of figures (part 2) 4.2, 4.8, 4.9, 4.10, 4.11 and 4.12a.